ARMY RESEARCH LABORATORY

Frontiers in Anisotropic Shock-Wave Modeling

by Alexander A. Lukyanov and Steven B. Segletes

ARL-TR-5878 February 2012

Approved for public release; distribution is unlimited.

NOTICES

Disclaimers

The findings in this report are not to be construed as an official Department of the Army position unless so designated by other authorized documents.

Citation of manufacturer's or trade names does not constitute an official endorsement or approval of the use thereof.

Destroy this report when it is no longer needed. Do not return it to the originator.

Army Research Laboratory

Aberdeen Proving Ground, MD 21005-5066

ARL-TR-5878 **February 2012**

Frontiers in Anisotropic Shock-Wave Modeling

Alexander A. Lukyanov

Abingdon Technology Centre, Schlumberger, Abingdon, OX14 1UJ, UK

Steven B. Segletes

Weapons and Materials Research Directorate, ARL

Approved for public release; distribution is unlimited.

REPORT DOCUMENTATION PAGE	Form Approved OMB No. 0704-0188

Public reporting burden for this collection of information is estimated to average 1 hour per response, including the time for reviewing instructions, searching existing data sources, gathering and maintaining the data needed, and completing and reviewing the collection information. Send comments regarding this burden estimate or any other aspect of this collection of information, including suggestions for reducing the burden, to Department of Defense, Washington Headquarters Services, Directorate for Information Operations and Reports (0704-0188), 1215 Jefferson Davis Highway, Suite 1204, Arlington, VA 22202-4302. Respondents should be aware that notwithstanding any other provision of law, no person shall be subject to any penalty for failing to comply with a collection of information if it does not display a currently valid OMB control number.
PLEASE DO NOT RETURN YOUR FORM TO THE ABOVE ADDRESS.

1. REPORT DATE *(DD-MM-YYYY)*	2. REPORT TYPE	3. DATES COVERED (From - To)
February 2012	Final	January 2011-October 2011

4. TITLE AND SUBTITLE	5a. CONTRACT NUMBER
Frontiers in Anisotropic Shock-Wave Modeling	5b. GRANT NUMBER
	5c. PROGRAM ELEMENT NUMBER

6. AUTHOR(S)	5d. PROJECT NUMBER
Alexander A. Lukyanov Steven B. Segletes	AH80
	5e. TASK NUMBER
	5f. WORK UNIT NUMBER

7. PERFORMING ORGANIZATION NAME(S) AND ADDRESS(ES)	8. PERFORMING ORGANIZATION REPORT NUMBER
Abingdon Technology Center, Schlumberger, Abingdon, OK14 1UJ, UK ; U.S. Army Research Laboratory, ATTN: RDRL-WMP-C, Aberdeen Proving Ground, MD 21005-5066	ARL-TR-5878

9. SPONSORING/MONITORING AGENCY NAME(S) AND ADDRESS(ES)	10. SPONSOR/MONITOR'S ACRONYM(S)
	11. SPONSOR/MONITOR'S REPORT NUMBER(S)

12. DISTRIBUTION/AVAILABILITY STATEMENT

Approved for public release; distribution is unlimited.

13. SUPPLEMENTARY NOTES

authors' email: aaluk@mail.ru, steven.b.segletes.civ@mail.mil
A. Lukyanov contact info: Tel.: +44 07840355383, Fax: +44 (0) 1234 758217.

14. ABSTRACT

Studies of anisotropic materials and the discovery of various novel and unexpected phenomena under shock loading has contributed significantly to our understanding of the behavior of condensed matter. The variety of experimental studies for isotropic materials displays systematic patterns, giving basic insights into the underlying physics of anisotropic shock-wave modeling. There are many similarities and significant differences in the phenomena observed for isotropic and anisotropic materials under shock-wave loading. Despite this, the anisotropic constitutive equations must represent, mathematically and physically, the generalization of the conventional constitutive equations for isotropic material and reduce to the conventional constitutive equations in the limit of isotropy. This report presents the current state of the art in the experimental and theoretical developments of this fascinating field.

15. SUBJECT TERMS

anisotropic material, anisotropic plasticity, shock waves, equation of state, stress decomposition

16. SECURITY CLASSIFICATION OF:			17. LIMITATION OF ABSTRACT	18. NUMBER OF PAGES	19a. NAME OF RESPONSIBLE PERSON
a. REPORT	b. ABSTRACT	c. THIS PAGE			Steven B. Segletes
Unclassified	Unclassified	Unclassified	UU	72	19b. TELEPHONE NUMBER (*Include area code*) 410-278-6010

Standard Form 298 (Rev. 8/98)
Prescribed by ANSI Std. Z39.18

Contents

List of Figures

List of Tables

Acknowledgment

The author (Lukyanov) thanks Prof. E. Romenski for many useful suggestions regarding shock-wave modeling. The discussions regarding the shock-wave experiments on a composite with Dr. J.C.F. Millett during the meetings at Cranfield University are also greatly appreciated. Both authors would like to thank Dr. Bryan Love for his thorough and thoughtful review of this report.

1. Introduction

Investigation of anisotropic material behavior (such as aluminum alloys, single crystals, composite materials, and laminated plates) has found significant interest in the research community due to the widespread application of anisotropic materials in aerospace and civil engineering problems. For example, aluminum alloys are one of the main materials in the construction of modern aircraft and rockets. The strain-rate-dependent mechanical behavior of anisotropic material (*e.g.*, aluminum alloys) in air and space vehicles is important for applications involving impact. These applications cover a wide range of situations such as crashworthiness and protective armours in air and space vehicles and other applications. Since shock-wave and high-strain-rate phenomena are involved in many physical phenomena, we are interested in understanding the material mechanical properties under these non-trivial conditions. This report presents the current state of the art in the experimental and theoretical developments of the shock-wave propagation in anisotropic solids, and more specifically, for anisotropic elastic-plastic solids.

This is a subject that has received considerable attention in the isotropic solid-state physics and mechanics literature in recent decades (*e.g.*, Wackerle [*1*]; Zel'dovich and Raizer [*2*]; Davison and Graham [*3*]; Eliezer *et al.* [*4*]; Asay and Shahinpoor [*5*]; Meyers [*6*]; Drumheller [*7*]). The impact loading of anisotropic materials is a subject that has received considerable attention for both low and high velocity in the recent monographs on composite materials (*e.g.*, Abrate [*8*], Reid and Zhou [*9*], Ryan *et al.* [*10*]) and in recent research papers on composite materials (*e.g.*, Hereil *et al.* [*11*], Bordzilovsky *et al.* [*12*], Dandekar *et al.* [*13*], Espinosa *et al.* [*14*], Millett *et al.* [*15*], Aktaş *et al.* [*16*], Hazell and Appleby-Thomas [*17*], García-Castillo *et al.* [*18*], Tekalur *et al.* [*19*]), research papers on metals (*e.g.*, Butcher [*20*], Johnson and Barker [*21*], Stevens and Tuler [*22*], Rosenberg *et al.* [*23, 24*], Gray III *et al.* [*25, 26*], Rubin [*27*]), and research papers on single crystals (*e.g.*, Winey and Gupta [*28–30*]).

To describe the anisotropic material response under shock loading, the following general aspects need to be investigated: appropriate constitutive equations to describe the strength effect and equations of state (EOSs) to describe the hydrodynamic behavior. Mechanical yielding and strength behavior in shock waves show complexities that are not understood yet, especially in anisotropic materials. Some approaches have been made by Johnson *et al.* (*31–33*), Segletes (*34*), O'Donoghue *et al.* (*35*), Anderson *et al.* (*36*), Winey and Gupta (*28–30*), and Lukyanov (*37–41*) to describe the constitutive relationships for an anisotropic material. The determination of the EOS

for anisotropic materials is an important problem in metallurgy, geophysics, aerospace, and also in other areas where the behavior of anisotropic materials at high pressures is of interest.

1.1 Experimental Framework

Modern, high-resolution methods for monitoring the stress and particle velocity histories in shock waves and equipment have been created (*e.g.*, Barker and Hollenbach [*42*]; Kanel [*43*]; Kanel *et al.* [*44*]; Millett and Bourne [*45*]; Bourne and Stevens [*46*]; Bourne [*47*]; Gu and Ravichandran [*48*]); numerous investigations into the mechanical properties of different classes of materials have been undertaken (*e.g.*, Meyers [*6*]; Gu and Ravichandran [*48*]; Steinberg [*49*]; Johnson *et al.* [*50*]; Kanel *et al.* [*51*]; Millett *et al.* [*52*]; Lopatnikov *et al.* [*53*]; Zaretsky *et al.* [*54*]; Gebbeken *et al.* [*55*]; Bronkhorst *et al.* [*56*]), and numerous phenomenological as well as microscopic models have been developed (*e.g.*, Wallace [*57*]; Swegle and Grady [*58*]; Steinberg [*49*]; Meyers [*6*]; Kanel *et al.* [*59*]; Nellis *et al.* [*60*]; Bourne and Gray III [*61*]; Krüger *et al.* [*62*]; Chijioke *et al.* [*63*]; Boidin *et al.* [*64*]; Petit and Dequiedt [*65*]). However, in spite of a perfectly adequate general understanding, experimental methodology, and theory, material models do not agree in detail, especially for anisotropic materials.

In the past, very few experimental results were published in the literature, either for anisotropic metals or composite materials. Only a few examples can be presented. For example, Whittier and Peck (*66*) measured the response due to low impact and studied the dispersion of the wave in unbounded layered media, not a laminated plate. Tauchert and Guzelsu (*67*) and Asay *et al.* (*68*) used ultrasonic methods to study dispersion and measure the "effective" elastic response of unbounded composites. The transient strain histories measurements were performed by Mortimer *et al.* (*69*) for fabricated graphite-epoxy plates (cross-ply layup and angle plies). Chhabildas and Swegle (*70, 71*) performed pressure-shear experiments, where the coupled longitudinal and transverse motion generated by the normal impact of Y-cut quartz is transmitted into an X-cut quartz, X-cut quartz, and alumina-filled epoxy samples.

Jones and Mote (*72*) presented experimental studies on shock propagation in a single crystal in copper including constitutive equations describing elastic precursor decay for wave propagation in the $\langle 100 \rangle$, $\langle 110 \rangle$, and $\langle 111 \rangle$ directions in fcc single crystals. Johnson *et al.* (*31*) proposed constitutive equations describing elastic precursor decay for longitudinal plane-wave propagation in fcc, bcc, and rocksalt structures with the wave propagation in the $\langle 100 \rangle$, $\langle 110 \rangle$, and $\langle 111 \rangle$ directions. Calculated theoretical results (Johnson *et al.* [*31*]) are compared with the experimental data on precursor amplitudes for single-crystal copper (fcc), tungsten (bcc), sodium chloride (NaCl) (rocksalt), and lithium fluoride (LiF) (rocksalt). Asay *et al.* (*73*) performed

experimental studies on shock propagation along a $\langle 100 \rangle$ direction in single-crystal LiF and showed that elastic precursor decay is critically dependent on the origin of the sample. Also, Gupta (*74*) presented experimental data for shock propagation along the $\langle 111 \rangle$ crystallographic direction in single-crystal LiF, with the observed elastic response up to 30 kbar experimental bounds and including shock propagation data along the $\langle 100 \rangle$, $\langle 110 \rangle$, and $\langle 111 \rangle$ directions (Gupta [*75*]). The dynamic elevated-temperature elastic properties of single-crystals and polycrystalline aluminum were studied by employing a laser pulse technique to produce propagating stress pulses in slender rods (Swearengen *et al.* [*76*]). The dynamic elastic-plastic of single crystal of the secondary explosive pentaerythritol tetranitrate (PETN) was studied by Halleck and Wackerle (*77*) at input shock strengths between 0.6 GPa for crystals with surfaces cut perpendicular to the $\langle 110 \rangle$ and $\langle 001 \rangle$ directions. Later, Dick and Ritchie (*78*) presented the measurements for the elastic precursor shock strength of pentaerythritol tetranitrate explosive crystals with $\langle 100 \rangle$, $\langle 101 \rangle$, $\langle 110 \rangle$, and $\langle 001 \rangle$ orientations. The measured precursor amplitudes were 0.38, 0.58, 0.98, and 1.22 GPa, respectively, for the four orientations.

However, this situation has changed recently for composite materials and single crystals, *i.e.*, a number of monograph and research papers were published (*e.g.*, Abrate [*8*]; Reid and Zhou [*9*]; Millett *et al.* [*15*]; Ryan *et al.* [*10*]; Aktaş *et al.* [*16*]; Hazell and Appleby-Thomas [*17*]; García-Castillo *et al.* [*18*]; Tekalur *et al.* [*19*]; Nurick *et al.* [*79*]; Iqbal *et al.* [*80*]; Enfedaque [*81*]; Panahia *et al.* [*82*]; Jackson and Shukla [*83*]). The major experimental methods were presented by Zhu and Lu (*84*) with a brief description of the corresponding experimental devices such as ballistic pendulums and a wide range of sensors to measure impulse, pressure, acceleration, and displacement of structures. The energy profile diagrams and associated load-deflection curves for a number of composite materials (*e.g.*, unidirectional glass/epoxy laminates, carbon fiber reinforced plastic [CFRP] laminates, woven carbon fiber/epoxy laminates) were obtained (Found and Howard [*85*]; Delfosse and Poursartip [*86*]; David-Westa [*87*]; Aktaş *et al.* [*16*]; Iqbal *et al.* [*80*]; Enfedaque [*81*]). New experimental data have been obtained for single crystals (*e.g.*, Asay [*88*]). A good overview of new development in the physical chemistry of shock compression was presented by Dlott (*89*).

For many years, it has been assumed in the shock-wave community that the response of materials to high intensity shock loading is isotropic, and only recently has anisotropy in the shock response attracted the attention of researchers (*e.g.*, Gupta [*75*], Dick and Ritchie [*78*], Gray III *et al.* [*25, 26*]). It was shown in an investigation of cold rolled and annealed zirconium (see Gray III *et al.* [*25*]) that the value of stresses varies in different directions in the quasi-static test and plate impact test. Gray III *et al.* (*26*) showed that under shock loading conditions (one-dimensional strain space), the variation of the Hugoniot elastic limit (HEL) or the yield strength of annealed

zirconium was consistent with the quasi-static experimental data. Previously, Butcher (*20*) worked on aluminum alloy 6061-T6 and predicted that spall strength should vary in accordance with the one-dimensional yield strength depending on material orientation. Chhabildas and Swegle (*70*) presented a technique to detect a 0.2 GPa shear wave in 6061-T6 aluminum alloy at 0.7 GPa longitudinal stress. Gupta (*75*) presented shock propagation data along the $\langle 100 \rangle$, $\langle 110 \rangle$, and $\langle 111 \rangle$ directions in LiF crystals where a marked anisotropy in wave profiles and in dynamic compressive strengths is observed. Here it is important to mention the work done by Johnson and Barker (*20*), Stevens and Tuler (*22*), and Rubin (*27*) on aluminum alloy 6061-T6 and Rosenberg *et al.* (*23, 24*) on the shock response of the alloy 2024-T86.

By their very nature, two-dimensional fiber composites are highly anisotropic. Eden *et al.* (*90*) used high-speed photography to investigate a quartz-phenolic resin composite. Bordzilovsky *et al.* (*12*) examined the effects of orientation to the shock axis of a unidirectional aramid fiber-epoxy composite, with the orientation of the fibers ranging from 5° to 90° to the shock axis. Work by Hereil *et al.* (*11*) on a three-dimensional carbon-carbon composite (in this case, the fibers and binder are orientated orthogonally) were in agreement with previous studies of Eden *et al.* (*90*). Millett *et al.* (*15*) studied the effect of fiber orientation on the shock response of a two-dimensional carbon fiber-epoxy composite (through thickness [fibers normal to the impact axis] and fiber at 0° [fibers parallel to the impact axis]) using the technique of plate impact.

A technique for the study of the behavior of metals under extreme conditions is the planar plate impact test (one-dimensional plane-strain shock-wave propagation). To describe the dynamic response of different materials under shock loading, the methodology based on the plate impact test is fundamental in the characterization of the Mie-Grüneisen EOS for isotropic materials by measuring shock velocity U_S and particle velocity u_p. The method was originally employed by Walsh and Christian (*91*) and later by many others (*e.g.*, McQueen and Marsh [*92*]; Van Thiel *et al.* [*93*]; Marsh [*94*]; Steinberg [*49*]; Meyers [*6*]; Trunin *et al.* [*95*]). Using U_S-u_p experimental data, further approximation of this experimental curve using equation 9 or 10 can be done. The same methodology can be used to validate the modified Mie-Grüneisen EOS for anisotropic materials; thus, a numerical simulation of the anisotropic plate impact test is considered.

In addition to its fundamental utility in characterizing the EOS, the plane shock-wave technique provides a powerful tool for studying material properties at different strain rates (*e.g.*, Kipp and Grady [*96*]; Steinberg [*49*]; Meyers [*6*]; Johnson *et al.* [*50*]; Kanel *et al.* [*51*]; Millett *et al.* [*52*]). Such characteristics as spall pressure, shock velocity, particle velocity, HEL, thickness of the spall section, time to spall, and free-surface velocity of the spall section can be measured and used for the characterization of material dynamic response (*e.g.*, Meyers [*6*]; Kanel *et al.* [*51*]; Kanel [*43*];

Krivtsov [*97*]; Millett *et al.* [*52*]; Bourne and Gray III [*61*]; and Stoffel [*98*]). In the earliest plane-wave experiments, two parameters that could be determined were the HEL (or stress level associated with the elastic precursor wave) and the dynamic compressibility (or bulk modulus) associated with the following plastic wave. More complex theories of material behavior have led to the extraction of much additional information from such experiments (definition of non-standard parameters, *e.g.*, Kiselev and Lukyanov [*99*]).

From an experimental point of view, it is clear that the production of waves in a metal target and the measurement of their characteristics, such as speed and intensity, provide one of the most convenient methods of investigating the physical properties of a material under high pressure. A schematic of the plate impact test is depicted in figure 1, in which a flyer plate impacts a target plate, which is bonded to a polymethylmethacrylate (PMMA) plate. In this report, the case is considered where the diameters of the flyer and the target are much greater than their thicknesses and the characteristic time of the process is the time of several runs of elastic waves across the thickness of the target plate. In such a case, the problem may be solved using a uniaxial strain state (one-dimensional mathematical formulation in strain space) and the adiabatic approximation; therefore, planar impact generates two one-dimensional shock waves. One propagates into the target and the other into the flyer plate. These shock waves reflect as rarefaction waves from the free surfaces of the flyer and from the back of target plates connected to the PMMA. With a thin flyer, these rarefaction waves interact inside the target, producing a state of tension in some regions, which leads to the spallation. A large set of spall experiments have been carried out by Kanel *et al.* (*100, 101*). In this work, the dynamic anisotropic elasto-plastic material behavior before spallation is considered.

The shock-wave experiment has certain potential advantages associated with the level of strain rate that can be induced and the commonly accepted belief that no geometrical dispersion effects occur. It has frequently provided the motivation for the construction of material constitutive relations and has been the principal means for determining material parameters for some of these relations (Steinberg [*49*]; Meyers [*6*]; Bourne and Gray III [*61*]; Chijioke *et al.* [*63*]; Gu and Ravichandran [*48*]).

1.2 Linear Anisotropic Constitutive Relationship

It is well known that elastic isotropic materials are characterized by two constants (Lamé parameters). In the case of anisotropic elastic material, the stiffness matrix is required to describe the constitutive relationship. The strain-stress constitutive relationship for any elastic material

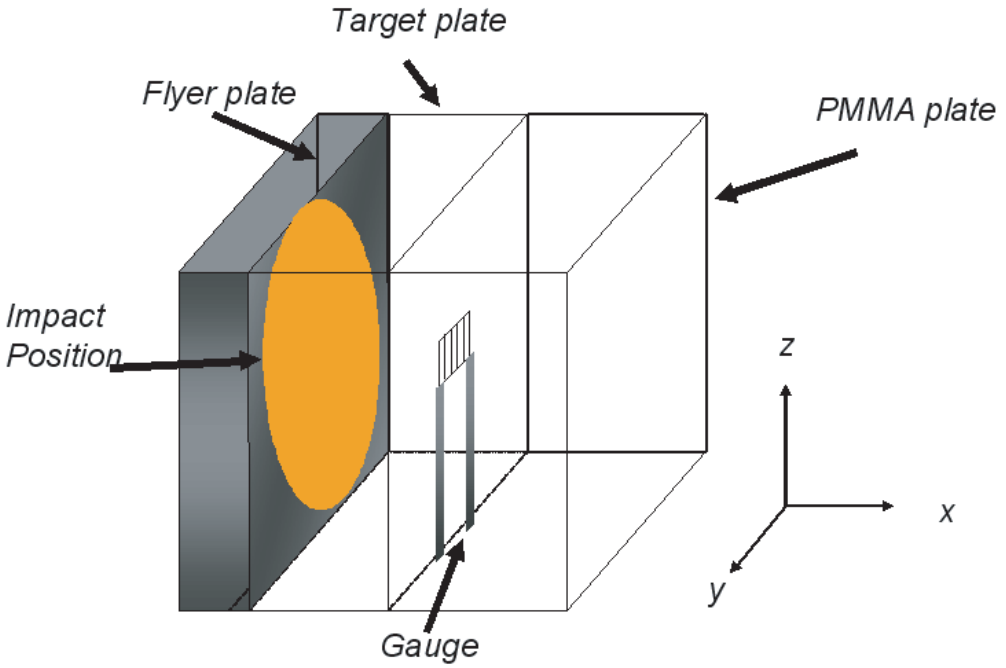

Figure 1. Schematic diagram of the experimental target assembly.

may be represented in contracted form as

$$\epsilon_{ij} = J_{ijkl}\sigma_{kl} \quad , \quad \sigma_{ij} = C_{ijkl}\epsilon_{kl} \quad , \quad C_{ijkl} = J^{-1}_{ijkl} \quad , \tag{1}$$

where C_{ijkl} are elements of the stiffness matrix and J_{ijkl} are elements of the compliance matrix. In this report, contraction by repeating indexes is assumed. In general, the stiffness matrix C_{ijkl} may be a function of σ_{ij}, ϵ_{ij}, $\dot{\epsilon}_{ij}$ and some other parameters. However, it is somewhat unwieldy as such, and is often considered to be constructed of constants, which produces the familiar Hooke's Law, equation 1. One reason why the deficiency of Hooke's Law becomes apparent experimentally under large pressures is that the bulk modulus of the material is quite different from the material's stress-free value. For isotropic materials, this problem has been solved by the introduction of conventional decomposition into two quantities: the hydrostatic stress (or pressure), which only induces a change of scale, and the deviatoric stress, which only induces a change of shape (*e.g.*, Wilkins [*102*]). This detailed description of such well-known facts will be used later in the construction of a generalized decomposition of the stress tensor, which will take into account physical properties of anisotropic materials. The pressure is defined as one-third the negative sum of the three normal stress components. For isotropic materials in the elastic region, the pressure is directly linked with volumetric strain, and the decomposition of the stress tensor

has the conventional form

$$\sigma_{ij} = -p\delta_{ij} + S_{ij} \quad , \quad p = -K\epsilon \quad , \quad S_{ij} = 2G\epsilon^d_{ij} \quad , \quad p = -\frac{1}{3}\left(\sigma_{11} + \sigma_{22} + \sigma_{33}\right) \quad , \tag{2}$$

where p is the hydrostatic pressure, S_{ij} is the deviatoric part of the stress tensor, K is the conventional bulk modulus, G is the shear modulus, δ_{ij} is the Kronecker delta symbol, $\epsilon^d_{ij} = \epsilon_{ij} - \frac{1}{3}\epsilon\delta_{ij}$ is the deviatoric strain tensor, and $\epsilon = \epsilon_{11} + \epsilon_{22} + \epsilon_{33}$ is the volumetric part of the strain tensor. The distortional change is represented by the deviatoric strain tensor ϵ^d_{ij}. Since experimental evidence reveals that the compressibility of many materials changes under large pressures, the deviatoric formulation suggests that while the simplicity of Hooke's Law (constant coefficients) might possibly be retained for computation of the deviatoric stresses and strains, a more accurate scalar EOS should simultaneously be employed to account for nonlinear compressibility effects.

2. Isotropic Shock-Wave Modeling

During moderate to high levels of shock loading, the material undergoes nonlinear behavior in which the deformation is thermodynamically coupled with the internal energy; therefore, an EOS is required to describe the material's response to these conditions. It is convenient in numerical codes to have an analytical form of the EOS, but such an analytic form is at best an approximation to the true relationship. The EOS for the computational treatment of isotropic materials typically defines the pressure as a function of density ρ (or specific volume, ν) and specific internal energy e. A very popular form of EOS that is used extensively for isotropic solid continua is the Mie-Grüneisen EOS:

$$p = f(\rho, e) = P_r(\nu) + \frac{\Gamma(\nu)}{\nu}\left(e - e_r(\nu)\right) \quad , \tag{3}$$

where ν is the specific volume and $\Gamma(\nu)$ is the Grüneisen gamma defined as

$$\Gamma(\nu) = \left(\frac{\partial p}{\partial e}\right)_{\nu} \quad . \tag{4}$$

Traditionally, Γ is taken to be constant $\Gamma = \Gamma_0$; alternatively, it has often been assumed that $\Gamma_0/\nu_0 = \Gamma(\nu)/\nu =$ constant in equation 3. Functions $P_r(\nu)$ and $e_r(\nu)$ are assumed to be known functions of ν on some reference curve. Possible reference curves include: the shock Hugoniot curve, a standard adiabatic curve (*e.g.*, the adiabatic through the initial state (p_0, ν_0)), the 0 K isotherm, the isobar $p = 0$, the curve $e = 0$, or some composite curve of one or more of the above

curves to cover the complete range of interest in the parameter ν. The most commonly used form of the Mie-Grüneisen EOS for solid materials, which uses the shock Hugoniot as the reference curve, is obtained by combining equation 3 with the Rankine-Hugoniot equations to obtain:

$$p = f(\rho, e) = P_H \cdot \left(1 - \frac{\Gamma}{2}\mu\right) + \rho\Gamma e \quad , \tag{5}$$

where P_H is the Hugoniot pressure, $\mu = \rho/\rho_0 - 1$ is the relative change of volume, Γ is the Grüneisen function, ρ is the density, ρ_0 is the initial density, e is the specific internal energy, and ν is the current specific volume. The shock Hugoniot is often preferred for the Mie-Grüneisen reference curve, precisely because the experimental data used to fit the EOS are shock-Hugoniot data. In this way, the Mie-Grüneisen reference curve need not be *derived from* the fitting data, but literally represents that data in terms of the P_H function. Furthermore, there is a perceived comfort in knowing that the computational trajectory of pressure *vs.* volume for an impact simulations will lie closer to the known reference Hugoniot curve than, for example, a cold curve.

The Rankine-Hugoniot equations for the shock jump conditions can be regarded as defining a relation between any pair of the ρ, p, e, u_p variables and U_S (Meyers [*6*]). In many dynamic experiments, u_p (the particle velocity directly behind the shock) and U_S (the velocity at which the shock wave propagates through the medium) are measured. Generally, the shock velocity U_S (and, by inference, the Hugoniot pressure) is a nonlinear function of particle velocity u_p and it is sometimes fit to the following polynomial relation (Steinberg [*49*]):

$$U_S = c + S_1 u_p + S_2 \left(\frac{u_p}{U}\right) u_p + S_3 \left(\frac{u_p}{U}\right)^2 u_p \quad . \tag{6}$$

This functional form is more often employed in the strictly linear form (with S_2 and S_3 identically zero). Kerley (*103*) shows that the linear U_S-u_p relationship, because of its wide acceptance, is often treated almost as a "law" rather than a fit. He explains that the general linearity observed in the U_S-u_p relationship arises because it is basically a "plot of u_p *vs.* itself," and that the linearity disappears when plotting the difference $U_S - u_p$ *vs.* u_p. Kerley's notation of a "plot of u_p *vs.* itself" refers to the fact that, considering U_S as the sum of u_p and $(U_S - u_p)$, the magnitude of $(U_S - u_p)$ is significantly smaller than that of u_p for strong shock. Since u_p *vs.* u_p is tautologically linear, the term $(U_S - u_p)$ therefore carries more concentrated EOS information than U_S alone, assuming one can measure it to as comparable an accuracy as U_S. Nonetheless, most shock-Hugoniot data fits are provided in this linear U_S *vs.* u_p form.

According to the constraints of Grüneisen theory, the Grüneisen parameter Γ must be a function

of volume alone. Many empirical forms have been proposed including

$$\Gamma = \frac{\gamma_0 + a\mu}{1+\mu} \quad . \tag{7}$$

This form reduces to the simpler fit, namely, $\nu/\Gamma =$ constant, mentioned earlier, for the case where a is zero. One must, however, be mindful of the compatibility of fits between the Hugoniot and Grüneisen functions. Segletes (*104–106*) has shown that arbitrary specification of shock-Hugoniot fits and Grüneisen fits can lead to thermodynamic instability of the EOS model.

Nonetheless, the Grüneisen EOS, if one adopts the cubic shock-velocity relation of equation 6, can be derived as

$$p = \frac{\rho_0 c^2 \mu \left[1 + \left(1 - \frac{\Gamma}{2}\right)\mu - \frac{\Gamma}{2}\mu^2\right]}{\left[1 - (S_1 - 1)\,\mu - S_2 \frac{\mu^2}{\mu+1} - S_3 \frac{\mu^3}{(\mu+1)^2}\right]^2} + (1+\mu)\cdot\Gamma\cdot E \quad , \tag{8}$$

when $\mu > 0$, and

$$p = \rho_0 c^2 \mu + (1+\mu)\cdot\Gamma\cdot E \quad , \tag{9}$$

when $\mu \leq 0$. In these equations, E is the internal energy per initial specific volume, c is the intercept of the U_S-u_p curve (nominally akin to the ambient bulk sound speed of the material, c_0), S_1, S_2, and S_3 are the coefficients of the slope of the U_S-u_p curve equation 6, γ_0 is the ambient Grüneisen gamma, and a is the first order volume correction to γ_0. Parameters c, S_1, S_2, S_3, γ_0, and a represent material properties, which define its EOS. Parameters have been defined to cover a large number of isotropic materials (Steinberg [*49*]). The tensile part of the EOS, equation 9, is outside the domain of the shock Hugoniot, but instead assumes a constant bulk modulus in the hydrostatic portion of the equation, along with Grüneisen energy coupling.

Other forms of the Mie-Grüneisen EOS have been put forth, based upon different assumptions regarding the reference curve and Grüneisen function, for example, a frequency-based approach (Segletes and Walters [*107*]; Segletes [*108, 109*]), in which the Mie-Grüneisen reference curve and the Grüneisen function are not independently specified, but rather are both interdependent functions of the characteristic frequency of the lattice, ω:

$$p\nu/\Gamma - E = \left(\frac{c_0}{\Gamma_0 \kappa}\right)^2 \left\{ \left[(\omega/\omega_0)^\kappa - 1 \right] + \kappa\,(\kappa - 1)\,(\omega/\omega_0)^\kappa \ln\left(\omega/\omega_0\right) \right\} \quad , \tag{10}$$

where the subscript 0 refers to a parameter at the ambient state, κ is a constant parameter defined

by

$$\kappa = [\Gamma_{\text{vol0}} - 1 + 3/2 \cdot \Gamma_0 \xi]/\Gamma_0 \quad , \tag{11}$$

c is the bulk sound speed, Γ_{vol} is the so-called "volumetric" Grüneisen parameter (*i.e.*, the Dugdale-MacDonald [*110*] definition), and the constant ξ, while defined by

$$\xi = 4/(3\Gamma_0) - d(\nu/\Gamma)/d\nu|_0 \quad , \tag{12}$$

is generally fit directly to EOS data (since $d\Gamma/d\nu$ is not easily measured).

Grüneisen theory indicates that the characteristic lattice vibrational frequency is related to the Grüneisen parameter by way of $\Gamma/\nu = (\partial p/\partial E)_\nu = -(d\omega/d\nu)/\omega$. Thus, by employing a preferred functional form for the volume-dependent lattice frequency,

$$\omega/\omega_0 = \left(3\Gamma_0\xi\left[(\nu_0/\nu)^{1/3} - 1\right] + 1\right)^{1/\xi} \quad , \tag{13}$$

the volume-dependent function for Γ may be obtained directly through differentiation of ω, thereby completely defining the EOS of equation 10 operationally in terms of p, E, and ν, given the five material constants defining the columns of table 1.

Table 1. EOS parameters for select materials.

	C_0 (m/s)	$1/\nu_0$ (kg/m^3)	Γ_0	Γ_{vol0}	ξ
Ag	3221	10490	2.22	2.29	0.500
Al	5189	2700	2.03	1.84	0.716
Cu	3995	8930	2.02	2.10	0.520
Stainless Steel	4571	7896	1.81	2.00	0.550

From the general EOS form of equation 10, expressions may be derived for the cold curve, p_c,

$$p_c = (C_0/\Gamma_0)^2 (\omega/\omega_0)^\kappa \ln(\omega/\omega_0)/\psi \quad , \tag{14}$$

as well as the Hugoniot,

$$p_H [\psi - (\nu_0 - \nu)/2] = \left(\frac{C_0}{\Gamma_0\kappa}\right)^2 \{ [(\omega/\omega_0)^\kappa - 1] + \kappa(\kappa - 1)(\omega/\omega_0)^\kappa \ln(\omega/\omega_0)\} \quad . \tag{15}$$

In both of these equations, the term $\psi = \nu/\Gamma$ is used as convenient shorthand. These curves may be compared to both diamond-anvil (essentially "cold" compression) and shock-Hugoniot data.

An example of such a comparison to aluminum, for two different levels of zoom, is given in figure 2. As can be seen from the nature of equations 14 and 15, there is no intrinsic way, through the selection of the parameters, to *independently* fit both cold and Hugoniot curves. That both curves, nonetheless, fit the data so well (and for a variety of different materials) is indicative of a more general suitability of the parent form described by equation 10.

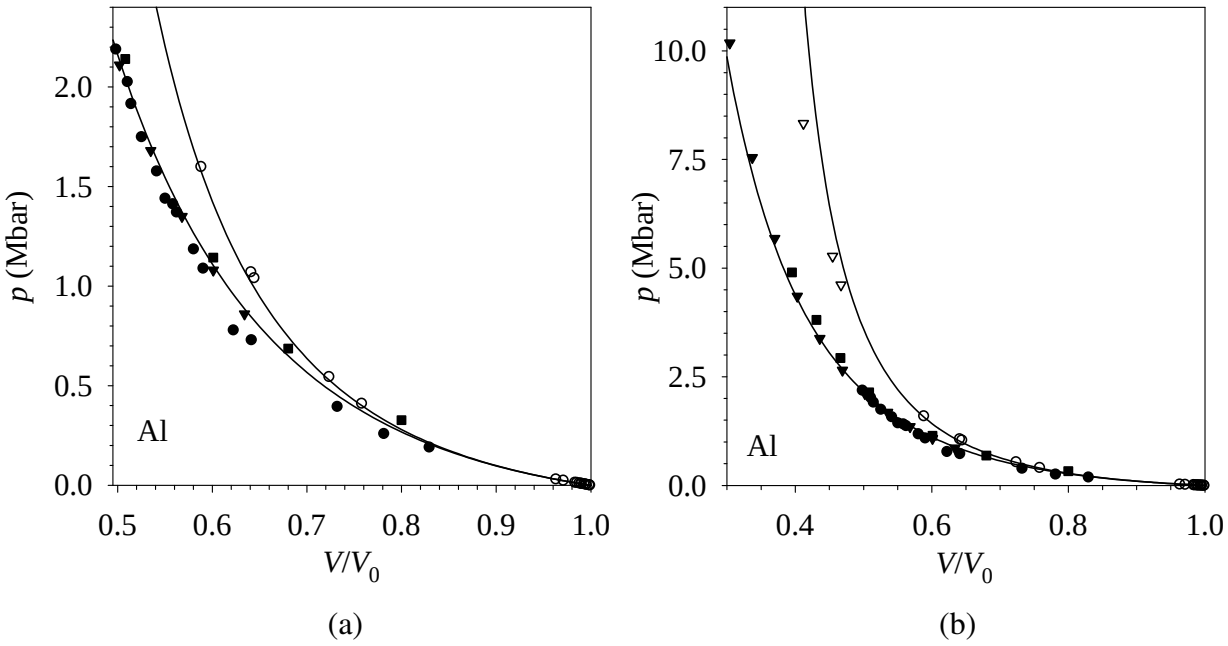

Figure 2. Cold-compression and shock-Hugoniot curves for aluminum (a) to 2.4 and (b) 11 megabars. Note that cold-compression data are filled symbols and Hugoniot data are open symbols.

3. Anisotropic Shock-Wave Modeling

Various models and numerical methods have been developed to simulate processes in solid media. The choice of these methods will depend largely on the problem and the available resources. A detailed review of the most common of these was provided by Benson (*111*).

3.1 Characteristics-based Solver

For modeling physical problems, such as high velocity impact and explosive loading of isotropic and anisotropic solid materials, there is strong demand on the numerical methods to simultaneously achieve high shock-wave resolution, maintain sharp interfaces, and accurately impose interfacial boundary conditions subject to finite deformation. A characteristics-based solver can be successfully used for solving the resulting hyperbolic partial differential equations (PDEs). Depending on the constitutive assumptions regarding the stress-strain relation, the resulting hyperbolic PDEs will have a different form (*i.e.*, different Lagrangian). Conservative formulations of the governing laws (PDEs) of elasto-plastic solid media have distinct advantages when solved using high-order shock capturing methods for simulating processes involving large deformations and shock waves. Let us define the density of Lagrangian L for our media, per unit initial volume, as

$$\begin{aligned} L &= \frac{1}{2}\rho_0\left(\mathbf{X}\right)\sum_i \dot{x}_i^2 - E\left(\mathbf{x},S\right) \\ E\left(\mathbf{x},S\right) &= E\left(\mathbf{X},\eta_{ij}^e,S\right) \\ E\left(\mathbf{x},S\right) &= \rho_0 e\left(\mathbf{x},S\right) \\ \eta_{ij}^e &= \frac{1}{2}\left(\sum_k F_{ki}^e F_{kj}^e - \delta_{ij}\right) \end{aligned} \quad , \tag{16}$$

where $\eta_{ij}^e = \eta_{ij}^e\left(\mathbf{X},t\right)$ are the elastic Lagrangian strains from $\mathbf{X}$ to $\mathbf{x}$, $\eta_{ij} = \eta_{ij}\left(\mathbf{X},t\right)$ are the total Lagrangian strains from $\mathbf{X}$ to $\mathbf{x}$, F_{kj}^e are elements of the elastic deformation gradient, F_{kj} are elements of the deformation gradient, and $E\left(\mathbf{x},S\right)$ is the density of internal energy per unit initial volume. Lagrange's equations of motion in the absence of body forces are

$$\frac{d}{dt}\frac{\partial L}{\partial \dot{x}_i} + \sum_k \frac{\partial}{\partial X_k}\frac{\partial L}{\partial F_{ik}^e} = 0 \tag{17}$$

or

$$\rho_0 (\mathbf{X}) \ddot{x}_i - \sum_k \frac{\partial}{\partial X_k} \left(\frac{\partial E}{\partial F^e_{ik}} \right)_S = 0 \quad . \tag{18}$$

Note that

$$\frac{\partial \eta_{lm}}{\partial F_{ik}} = \frac{1}{2} \left(F_{il} \delta_{km} + F_{im} \delta_{kl} \right) \quad , \quad \frac{\partial \eta^e_{lm}}{\partial F^e_{ik}} = \frac{1}{2} \left(F^e_{il} \delta_{km} + F^e_{im} \delta_{kl} \right) \quad . \tag{19}$$

With equation 19, and noting the symmetry of η_{ij} and η^e_{ij}, the equation of motion equation 18 is

$$\rho_0 (\mathbf{X}) \ddot{x}_i = \sum_k \frac{\partial}{\partial X_k} \left(\sum_l F^e_{il} \left(\frac{\partial E}{\partial F^e_{kl}} \right)_S \right) \quad . \tag{20}$$

A characteristics-based solver can be applied when the system equation 20 is closed by analytical formulae for the specific internal energy $e(\mathbf{x}, S)$. For small-amplitude elastic anisotropic wave propagation ($\eta^e_{ij} = \eta_{ij}$), specific internal energy can be written as quadratic form:

$$\rho e (\mathbf{x}, S) = \frac{1}{2} \eta_{ij} C^S_{ijkl} \eta_{kl} + TS \quad . \tag{21}$$

For isothermal motion, the potential in the Lagrangian density L is the density of free energy $F(\mathbf{x}, S) = F\left(\mathbf{X}, \eta^e_{ij}, S\right)$ per unit initial density in place of $E(\mathbf{x}, S) = E\left(\mathbf{X}, \eta^e_{ij}, S\right)$, and the adiabatic elastic constants C^S_{ijkl} are then isothermal C^T_{ijkl}. In the case of isotropy, an isentropic hyperelastic EOS in terms of the invariants of the elastic Greens tensor was considered (Miller and Colella [*112*]; Barton *et al.* [*113*]):

$$\begin{aligned} & e(J_1, J_3) = -\int_{\nu_0}^{\nu} P(\nu)\, d\nu + \frac{G}{2\rho_0} \left(J_1 - 3 J_3^{1/3} \right) \\ & J_1 = \mathrm{tr}\,(\mathbf{C}) \\ & J_2 = \frac{1}{2} \left[(\mathrm{tr}\,\mathbf{C})^2 - \mathrm{tr}\,\mathbf{C}^2 \right] \\ & J_3 = \det |\mathbf{C}| \end{aligned} \quad , \tag{22}$$

where $\mathbf{C} = (\mathbf{F}^e)^T \mathbf{F}^e$ is the elastic Green's tensor. The quantity $P(\nu)$ can be described by any form of isotropic EOS. Another form of the isotropic hyperelastic EOS has been put forth (Dorovskii *et al.* [*114*]; Barton *et al.* [*113*]; Barton and Drikakis [*115*]):

$$e(J_1, J_2, J_3, S) = \frac{K_0}{2\alpha^2} \left(J_3^{\alpha/2} - 1 \right)^2 + c_\nu T_0 J_3^{\gamma/2} \left(\exp\left[S/c_v \right] - 1 \right) + \frac{B_0}{2} J_3^{\beta/2} \left(J_1^2/3 - J_2 \right) \quad , \tag{23}$$

where $J_1 = \text{tr}\,(\mathbf{C}_F)$, $J_2 = \frac{1}{2}\left[(\text{tr}\,\mathbf{C}_F)^2 - \text{tr}\,\mathbf{C}_F^2\right]$, and $J_3 = \det|\mathbf{C}_F|$ are the invariants corresponding to the elastic Finger tensor $\mathbf{C}_F = (\mathbf{F}^e)^{-T}(\mathbf{F}^e)^{-1}$. The parameters $K_0 = c_0^2 - \left(\frac{4}{3}\right) b_0^2$, $B_0 = b_0^2$ are the squared bulk speed of sound and the squared speed of shear waves, respectively; c_v is the heat capacity at constant volume; and α, β, γ are constants characterizing the nonlinear dependence of sound speeds and temperature on the mass density. The specific internal energy can be decomposed into potentials describing the cold compression, $e_c\,(\rho, S)$; thermal energy density, $e_t\,(\rho, S)$; and the contribution due to shear strain, $e_s\,(\mathbf{F}^e, S)$. A more general function might also include a contribution due to changes in dislocation density, $e_h\,(\mathbf{F}^e, S)$ (Schreyer and Maudlin [*116*]). Thus, a general form could be written

$$e\,(\mathbf{F}^e, S) = e_c\,(\rho, S) + e_t\,(\rho, S) + e_s\,(\mathbf{F}^e, S) + e_h\,(\mathbf{F}^e, S) \quad . \tag{24}$$

High-order shock capturing methods, based upon solving Riemann problems locally at each cell edge throughout a computational domain, have emerged as a favorable approach to meeting the shock-wave modeling requirements. Recently, a high-order shock capturing scheme was proposed for solid dynamics where Godunov's method was applied to an Eulerian model (Godunov and Romenskii [*117*]) in conservative form using fixed Cartesian grids (Miller and Colella [*112*]; Barton *et al.* [*113*]; Barton and Drikakis [*115*]). Application of these numerical methods to solid mechanics has been made possible by formulations of the governing theory as first-order hyperbolic systems of conservation laws in the Eulerian frame (Godunov and Romenskii [*117*]; Kondaurov [*118*]; Plohr and Sharp [*119*]; Godunov and Romenski [*120*]). Introducing the vector of primitive variables W, equation 20 can be rewritten as a quasi-linear system naturally suitable for a characteristics-based solver:

$$\frac{\partial W}{\partial t} + A^\alpha \frac{\partial W}{\partial x^\alpha} = Q^p \quad , \tag{25}$$

where Q^p is the vector related to irreversible processes within the system. In the ensuing computational method, the convective flux terms in equation 20 are usually discretized using the well-known method of Godunov. The solution is therefore required of a local Riemann problem at the boundaries of each cell in the computational mesh. The solution is found using an approximate method based upon the characteristic tracing and thus requires detailed knowledge of the eigen-values and the eigenvectors of equation 20.

The method of characteristics was successfully used to demonstrate the accuracy of the lamination theory (Whitney and Pagano [*121*]) in transient wave propagation problems for anisotropic materials. This method is adequate for stiff materials or weak shocks where the

compression is small and the elastic response is nearly linear. The laminated plate equations used in this report are those derived by Whitney and Pagano (*121*), which are considered as a representative "first-order" laminated plate theory. Note that several analytical and numerical solutions to the laminated plate equations were constructed in the past. For example, Wang and Tuckmantal (*122*), and Moon (*123*) have discussed the wave surface based on the laminated plate equations due to abrupt change in stress. Also, Chow (*124*) applied the Laplace transform technique and calculated the deflection of a laminated plate under a concentrated load. Moon (*123*) solved the problem of one-dimensional wave propagation due to a prescribed line load by the fast Fourier transform technique. Furthermore, Sun and Lai (*125*) analyzed the response of a unidirectional fiber-reinforced layer subjected the response of a unidirectional fiber-reinforced layer subject to the laminated plate equations and exact equations. For symmetric cross-ply, or balanced angle-ply, laminated plates under one-dimensional in plate impact, the resulting hyperbolic partial differential equations (Whitney and Pagano [*121*]) reduce to (Mortimer *et al.* [*69*])

$$A_{11}\nabla^2 u^0\left(\mathbf{x},t\right) = M\frac{\partial^2 u^0\left(\mathbf{x},t\right)}{\partial t^2} \quad , \tag{26}$$

where $\mathbf{x}$ represents the spatial coordinate in the direction of wave propagation, t the time coordinate, $u^0\left(\mathbf{x},t\right)$ the mid-plane displacements in the $\mathbf{x}$-direction, and $M$the plate mass term. This is a simple wave equation with wave velocity $c_0 = \left(A_{11}/M\right)^{1/2}$. For a finite length striker plate of the same material as the specimen, the response in the specimen is simply a rectangular wave of amplitude $\epsilon_0 = V_0/(2c_0)$ and pulse length $t_0 = 2l/c_0$, where ϵ_0 is the strain, V_0 the initial velocity of the striker, and l is the length of the striker.

For symmetric cross-ply, or balance angle-ply, laminated plates under one-dimensional transverse shear-bending impact, the governing equations (without surface tractions) reduce to

$$kA_{55}\left(\nabla\psi_x + \nabla^2 w\right) = M\frac{\partial^2 w}{\partial t^2} \quad , \tag{27}$$

$$D_{11}\nabla^2\psi_x + D_{16}\nabla^2\psi_y - kA_{55}\left(\psi_x + \nabla w\right) = I\frac{\partial^2\psi_x}{\partial t^2} \quad , \tag{28}$$

$$D_{16}\nabla^2\psi_x + D_{66}\nabla^2\psi_y - kA_{44}\psi_y = I\frac{\partial^2\psi_y}{\partial t^2} \quad , \tag{29}$$

where the A_{ij}, D_{ij}, and I are plate coefficients as defined in Whitney and Pagano (*121*); w, ψ_x, ψ_y the specimen deflection and rotations, respectively; and k the shear correction factor. These equations 27–29 are a set of totally hyperbolic partial differential equations and were successfully solved by a numerical method of characteristics by Mortimer *et al.* (*69*).

3.2 Nonlinear Anisotropic Elastic Incremental Formalism

In the early 1970s, Johnson *et al.* (*31–33*) developed a continuum framework for describing the rate dependent elastic-plastic response of single crystals to shock-wave loading. Their tensor formulation coupled linear elastic response to a dislocation dynamics model that incorporated the appropriate slip system in the shocked crystals. In this framework, both elastic and plastic anisotropy were explicitly accounted for. This approach, similar to the above method of characteristics, is adequate for stiff materials or weak shocks, where the compression is small and the elastic response is nearly linear. However, for more compliant materials, crystals, or stronger shocks, several factors must be accounted for: (1) large compressions lead to a nonlinear elastic response, (2) low yield stresses lead to large deformations, and (3) large compressions and large plastic deformations lead to a significant temperature increase. As a result, to address these complications, Winey and Gupta (*28–30*) developed a consistent Lagrangian thermomechanical framework for modeling the response of a single crystal under shock loading. This framework is also applicable for anisotropic materials, highly anisotropic materials such as molecular crystals, and strong shocks in other single crystals. The Winey and Gupta (*28–30*) approach is constructed on the thermodynamic approach of Wallace (*126, 127*), which couples nonlinear elasticity within a thermodynamically consistent incremental formalism. In this method, the incremental displacement from some intermediate configuration x_i^n at time n to the next configuration x_i^{n+1} at time $n+1$,

$$(u_i)_n^{n+1} = x_i^{n+1} - x_i^n \quad , \tag{30}$$

where $(u_i)_n^{n+1}$ denotes the displacement at time $n+1$ relative to time n. The incremental strains (negative in compression), given by

$$\Delta\epsilon_{ij} = \frac{1}{2}\left[\frac{\partial\,(u_i)_n^{n+1}}{\partial x_j^n} + \frac{\partial\,(u_j)_n^{n+1}}{\partial x_i^n}\right] \quad , \tag{31}$$

are measured relative to the configuration at time n. The reference configuration is updated from the current configuration to the next configuration after every strain increment. The incremental

equations for internal energy (Gibbs equality) are

$$E^{n+1} - E^n = \frac{1}{\rho^n} \left(t_{ij}\right)_n^{n+1/2} \Delta\epsilon_{ij} + T^{n+1/2}\Delta S$$

$$\left(t_{ij}\right)_n^{n+1/2} = \frac{1}{2}\left[\left(t_{ij}\right)_n^{n+1} + \left(t_{ij}\right)_n^{n}\right] \quad , \tag{32}$$

$$T^{n+1/2} = \frac{1}{2}\left[T^{n+1} + T^{n}\right]$$

where ρ^n is the density for the reference configuration at time n; T^{n+1} and T^n are the temperature of the configuration at time $n+1$ and n, respectively; and $\left(t_{ij}\right)_n^{n+1}$ and $\left(t_{ij}\right)_n^{n}$ are the thermodynamic stresses for configuration at time $n+1$ and n, respectively. The thermodynamic definitions of temperature and stress tensor are defined by

$$T^n = \left[\frac{\partial E^n}{\partial S}\right]_{\epsilon_{ij}} \quad , \quad \left(t_{ij}\right)_n^{n+1} = \rho^n \left[\frac{\partial E^{n+1}}{\partial \epsilon_{ij}}\right]_S \quad . \tag{33}$$

Similar to Wallace (*126*), the anisotropic Grüneisen tensor was defined by Winey and Gupta (*28–30*):

$$\left(\Gamma_{ij}\right)_n^n = -\frac{1}{\rho^n T^n}\left[\frac{\partial \left(t_{ij}\right)_n^{n+1}}{\partial S}\right]_S \quad . \tag{34}$$

Therefore, the incremental change in the thermodynamic stresses, using the EOS equation 34, is

$$\left(t_{ij}\right)_n^{n+1} - \left(t_{ij}\right)_n^{n} = \left(C_{ijkl}\right)_n^{n+1/2} \Delta\epsilon_{kl} - \rho^n \left(\Gamma_{ij}\right)_n^{n+1/2} T^{n+1/2}\Delta S \quad , \tag{35}$$

where the linear elastic coefficients are defined by

$$\left(C_{ijkl}\right)_n^n = \left[\frac{\partial \left(t_{ij}\right)_n^n}{\partial \epsilon_{kl}}\right]_S \quad . \tag{36}$$

In the Winey and Gupta (*28*) approach, the elastic coefficients in equation 36 are functions of strain and entropy. As a result, the incremental change from configuration at time n to configuration at time $n+1$ is

$$\left(C_{ijkl}\right)_n^{n+1} - \left(C_{ijkl}\right)_n^{n} = \left[\left(\frac{\partial C_{ijkl}}{\partial \epsilon_{mn}}\right)_S\right]_n^{n+1/2} \cdot \Delta\epsilon_{mn} + \left[\left(\frac{\partial C_{ijkl}}{\partial S}\right)_{\epsilon_{ij}}\right]_n^{n+1/2} \cdot \Delta S \quad , \tag{37}$$

$$\left(C_{ijklmn}\right)_n^n = \left[\left(\frac{\partial C_{ijkl}}{\partial \epsilon_{mn}}\right)_S\right]_n^n$$

where nonlinear elastic coefficients C_{ijklmn} are assumed to be independent of strain and entropy in this formulation, so that $(C_{ijklmn})_n^{n+1} = (C_{ijklmn})_n^n$. To maintain thermodynamic consistency, the Winey and Gupta (*28*) approach assumes for derivatives that

$$\left[\frac{\partial C_{ijkl}}{\partial S}\right]_{\epsilon_{ij}} = -\rho \left[\frac{\partial \left(T\Gamma_{ij}\right)}{\partial \epsilon_{kl}}\right]_S \quad . \tag{38}$$

In general, Γ_{ij} is a function of entropy and strain. However, for simplicity, the Winey and Gupta (*28*) approach assumes Γ_{ij} to be constant. Hence,

$$\left[\frac{\partial C_{ijkl}}{\partial S}\right]_{\epsilon_{ij}} = -\rho\Gamma_{ij}\left[\frac{\partial T}{\partial \epsilon_{kl}}\right]_S = \rho T\Gamma_{ij}\Gamma_{kl} \tag{39}$$

When equation 39 is substituted into equation 37, the incremental change in the linear elastic coefficients under the Winey and Gupta (*28*) assumptions can be written as

$$(C_{ijkl})_n^{n+1} - (C_{ijkl})_n^n = (C_{ijklmn})_n^{n+1/2} \cdot \Delta\epsilon_{mn} + \rho^n T^{n+1/2} \left(\Gamma_{ij}\right)_n^{n+1/2} \left(\Gamma_{kl}\right)_n^{n+1/2} \cdot \Delta S \quad . \tag{40}$$

To complete the thermodynamic description, the temperature increment from configuration at time n to configuration at time $n+1$ is given by

$$T^{n+1} - T^n = -T^{n+1/2} \left(\Gamma_{ij}\right)_n^{n+1/2} \Delta\epsilon_{ij} + \left(\frac{T}{c_\epsilon}\right)^{n+1/2} \Delta S \quad , \tag{41}$$

where c_ϵ is the specific heat capacity at constant elastic configuration. To maintain consistency with constant Γ_{ij}, it is assumed that c_ϵ is to be constant as well. It is important to note that in this formulation, the thermodynamic stresses, elastic coefficients, and other tensor properties must be updated during the incremental calculation so that they are referred to the configuration at time n.

Using the above framework, the propagation of large amplitude stress waves along the arbitrary directions in quartz, sapphire, LiF, copper single crystal, and unreacted PETN are performed by Winey and Gupta (*28–30*). Measured (Asay *et al.* [*73*]) and simulated (Winey and Gupta [*29*]) longitudinal stress histories for LiF single crystals shocked along the $\langle 100 \rangle$ orientation are presented in figure 3. They have also discussed differences between pure mode wave propagation for linear and nonlinear elastic deformation.

3.3 Conventional Decomposition of Anisotropic Equations

Speaking generally, any second-order tensor can be decomposed into the spherical part and the deviatorical part. In the case of continuum mechanics, the decomposition of the stress tensor and

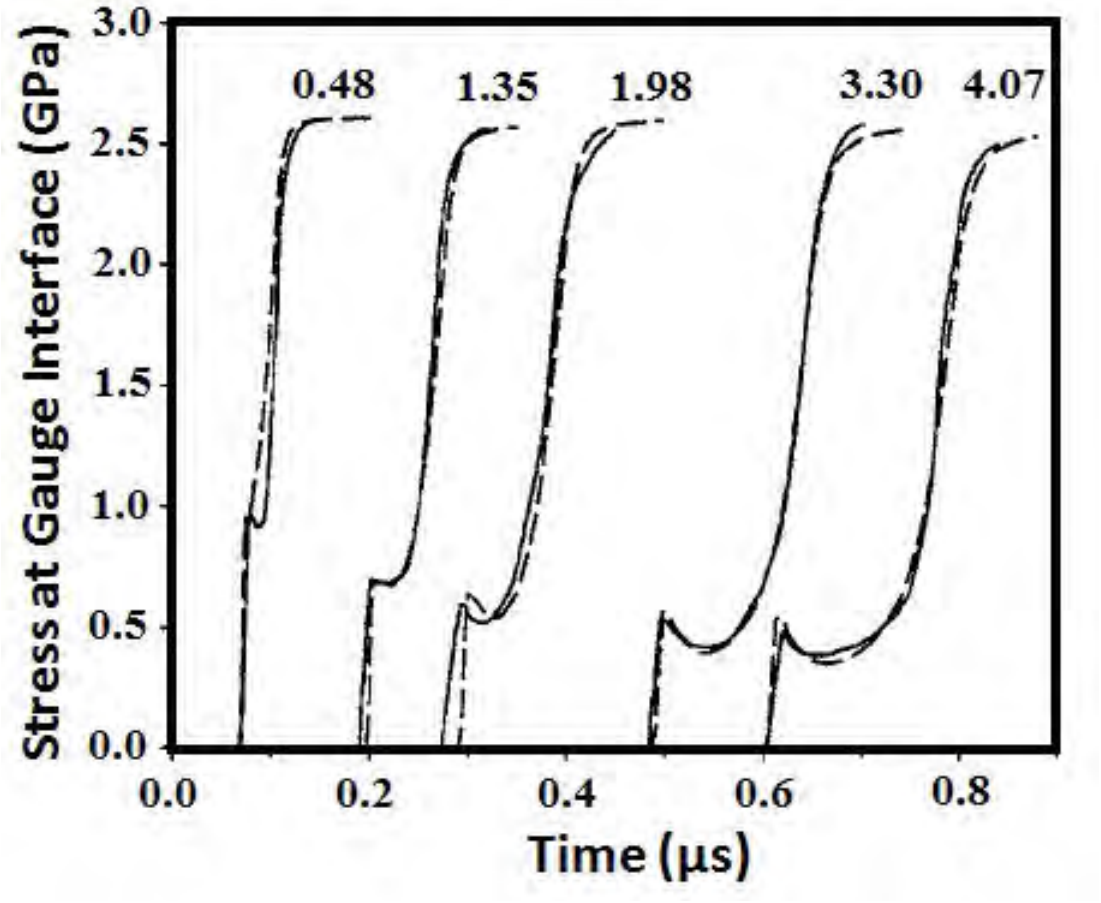

Figure 3. Measured (solid lines) and simulated (dashed lines) longitudinal stress histories for LiF single crystals shocked along the $\langle 100 \rangle$ orientation. The experimental data (Asay *et al.*) (*73*) and simulations (Winey and Gupta) (*29*) are for a 6061-T6 aluminum plate impacting the LiF crystals at a velocity of *ca.* 0.34 km/s, where the target crystals are backed by a quartz stress gauge. The stress is measured at the interface between the LiF crystal and the quartz gauge. The numbers above the curves indicate the sample thickness in mm. Time is relative to the moment of impact. Reprinted with permission from Winey, J.M., Gupta, Y. M., *J. Appl. Phys.* **99**, 023510, (2006). Copyright 2006, American Institute of Physics.

the strain tensor into their volumetric and deviatoric components (*e.g.*, Wilkins [*102*]) has certain physical justification. This step is done in order to distinguish between thermodynamic (EOS) response and the ability of the material to carry shear loads (strength). For anisotropic materials, the decomposition of the stress and strain tensors into spherical and deviatoric parts in stress space and strain space results in stress and strain components that do not correspond to each other due to the material properties' anisotropy. For example, using the stress-strain relation for an orthotropic material, the hydrostatic pressure can be rewritten as

$$\begin{aligned} p = & \frac{-1}{9\beta}\left\{E_1(1-\nu_{23}\nu_{32}) + E_2(1-\nu_{13}\nu_{31}) + E_3(1-\nu_{12}\nu_{21})\right. \\ & \left. +2\cdot[E_1(\nu_{21}+\nu_{31}\nu_{23}) + E_1(\nu_{31}+\nu_{21}\nu_{32}) + E_2(\nu_{32}+\nu_{31}\nu_{12})]\right\}\cdot\epsilon \\ & -\frac{1}{3\beta}\left\{E_1(1-\nu_{23}\nu_{32}) + E_1(\nu_{21}+\nu_{31}\nu_{23}) + E_1(\nu_{31}+\nu_{21}\nu_{32})\right\}\cdot\epsilon_{11}^d \\ & -\frac{1}{3\beta}\left\{E_1(\nu_{21}+\nu_{31}\nu_{23}) + E_2(1-\nu_{13}\nu_{31}) + E_2(\nu_{32}+\nu_{12}\nu_{31})\right\}\cdot\epsilon_{22}^d \\ & -\frac{1}{3\beta}\left\{E_1(\nu_{31}+\nu_{21}\nu_{32}) + E_2(\nu_{32}+\nu_{12}\nu_{31}) + E_3(1-\nu_{12}\nu_{21})\right\}\cdot\epsilon_{33}^d \end{aligned} \quad , \tag{42}$$

where $\beta = 1-\nu_{12}\nu_{21}-\nu_{13}\nu_{31}-\nu_{23}\nu_{32}-2\nu_{21}\nu_{32}\nu_{13}$, E_1, E_2, E_3 are the Young's moduli, and ν_{ij} are the six Poisson ratios. Hence, for an anisotropic material in general, the mean stress depends on the deviatoric strains and, as a result, the decomposition used for isotropic materials is not applicable.

3.4 Deviatoric Constitutive Relationship for Anisotropic Materials

While the mathematics and physics of the constant coefficient constitutive relationship for isotropic materials was well understood, the casting of these rules into an anisotropic framework was not a straightforward task. In particular, the difficulties were associated with two primary differences in the behavior of anisotropic materials with respect to that of isotropic materials: (1) under hydrostatic pressure, strain is not uniform in all three directions of the material coordinates, and (2) except under restrictive modulus conditions, deviatoric stress will produce volumetric dilatation. As a solution of these difficulties, the elastic generalized deviatoric anisotropy decomposition was proposed by Segletes (*34*). While his arguments were applied to the case of transversely isotropic materials, the generalization to orthotropy is straightforward and is shown directly. Decomposition of the stress and strain tensors into their hydrostatic and generalized deviatoric components yields (Segletes [*34*])

$$S_{ij} = \sigma_{ij} - \sigma\delta_{ij} \quad , \quad S_{ij}\delta_{ij} = 0 \quad , \quad \sigma = \frac{1}{3}\left(\sigma_{11}+\sigma_{22}+\sigma_{33}\right) \quad , \tag{43}$$

$$e_{ij} = \epsilon_{ij} - \bar{\epsilon}_{ij} \quad , \tag{44}$$

$$\bar{\epsilon}_{ij} = \sigma J_{ijkl} \delta_{kl} \quad , \tag{45}$$

$$e_{ij}\delta_{ij} = \bar{e} \neq 0 \ , \quad \frac{3\delta_{ij}\, C_{ijkl}\, \epsilon^{d}_{ij}}{\delta_{ij}\, C_{ijkl}\, \delta_{kl}} = \bar{\epsilon} \neq 0 \quad . \tag{46}$$

where σ is the hydrostatic stress, $\bar{\epsilon}_{ij}$ represents the normal strains due to hydrostatic stress, $\bar{e}$ is the dilation of generalized deviatoric strain, and $\bar{\epsilon}$ is the excess anisotropic dilation. One may acquire upon substitution into equations 43–45

$$S_{ij} + \sigma\delta_{ij} = C_{ijkl}e_{kl} + C_{ijkl}\bar{\epsilon}_{kl} \quad . \tag{47}$$

Unlike the isotropic materials in which a hydrostatic pressure produces a uniform dilatation in all three coordinate directions, hydrostatic strain for an anisotropic material is non-uniform. Therefore, if one defines the deviatoric components of stress and strain to be the total stress / strain components decremented by an amount that would result from a hydrostatic stress state, one can conclude (per condition (1) above) that there is a unique hydrostatic strain component associated with all three directions in the material coordinates (the coordinate system that produces no shear coupling). Equation 47 may be decoupled to give a hydrostatic equation,

$$\sigma\delta_{ij} = C_{ijkl}\bar{\epsilon}_{kl} \quad , \tag{48}$$

and a deviatoric relationship void of hydrostatic terms

$$S_{ij} = C_{ijkl}e_{kl} \quad . \tag{49}$$

Under the influence of a purely hydrostatic stress state (and assuming the moduli to be constant), there will be constant ratios between the components of normal strains $\bar{\epsilon}_{ij}$ due to hydrostatic stress. Defining the ratios in terms of material compliances J_{ijkl}, it follows from equation 45 that

$$\frac{\bar{\epsilon}_{11}}{\bar{\epsilon}_{22}} = K^{\epsilon}_{12} = \frac{J_{1111} + J_{1122} + J_{1133}}{J_{2211} + J_{2222} + J_{2233}} \ , \quad \frac{\bar{\epsilon}_{33}}{\bar{\epsilon}_{22}} = K^{\epsilon}_{32} = \frac{J_{3311} + J_{3322} + J_{3333}}{J_{2211} + J_{2222} + J_{2233}} \quad . \tag{50}$$

Recall from equation 46 that the sum of the three normal deviatoric strain increments is not generally zero, but rather equals a deviatoric dilatation, $\bar{e}$. The significance of this term is that a state of stress whose average normal value is zero can produce volumetric change on an element with respect to that element's stress free volume. We may substitute the normal components of equation 44 into equation 46 and, with the aid of equation 50, develop a relation between $\bar{e}$ and $\bar{\epsilon}_{22}$:

$$\bar{\epsilon}_{22} = \frac{(\epsilon_{11} + \epsilon_{22} + \epsilon_{33}) - \bar{e}}{K^{\epsilon}_{12} + 1 + K^{\epsilon}_{32}} \quad . \tag{51}$$

Likewise, one may employ the condition of uniform strain ($\epsilon_{11} = \epsilon_{22} = \epsilon_{33}$) into the deviatoric constitutive relation, equation 49, to acquire constant ratios between the components of normal stresses resulting from the uniform strain state:

$$\frac{\sigma_{11}}{\sigma_{22}} = K_{12}^{\sigma} = \frac{C_{1111} + C_{1122} + C_{1133}}{C_{2211} + C_{2222} + C_{2233}} \quad , \quad \frac{\sigma_{33}}{\sigma_{22}} = K_{32}^{\sigma} = \frac{C_{3311} + C_{3322} + C_{3333}}{C_{2211} + C_{2222} + C_{2233}} \quad . \tag{52}$$

So as to insure that the deviatoric stress has no hydrostatic component, substitute equation 49 into equation 43, in light of equation 52, to show that

$$K_{12}^{\sigma} e_{11} + e_{22} + K_{32}^{\sigma} e_{33} = 0 \quad . \tag{53}$$

From this equation, $e_{11} + e_{22} + e_{33}$ may be isolated and replaced with $\bar{e}$, and the remaining e_{ij} terms eliminated via equation 44, eventually producing a second relation between $\bar{e}$ and $\bar{\epsilon}_{22}$:

$$\bar{\epsilon}_{22} = \frac{\bar{e} + (K_{12}^{\sigma} - 1)\epsilon_{11} + (K_{32}^{\sigma} - 1)\epsilon_{33}}{K_{12}^{\epsilon}(K_{12}^{\sigma} - 1) + K_{32}^{\epsilon}(K_{32}^{\sigma} - 1)} \quad . \tag{54}$$

The $\bar{\epsilon}_{22}$ term may be eliminated between equations 51 and 54 to produce a closed-form for $\bar{e}$ in terms of the current strain state ϵ_{ij} and the material parameters K_{ij}^{σ} and K_{ij}^{ϵ}. Once $\bar{e}$ is obtained, $\bar{\epsilon}_{22}$ follows from either equation 51 or 54. The other $\bar{\epsilon}_{ij}$ components follow from equation 50, and finally, from equation 44, the deviatoric strain terms e_{ij} follow. All unknown deviatoric strains are now solved. As an aside, to recreate the transversely isotropic condition described by Segletes (*34*), the terms K_{32}^{σ} and K_{32}^{ϵ} need merely be set equal to unity.

Summing the three equations for normal stress equation 48 subject to equations 44 and 46 yields upon reduction

$$\sigma = \tilde{K}^{\sigma} \left(\epsilon_{11} + \epsilon_{22} + \epsilon_{33} + \bar{\epsilon} \right) \quad , \tag{55}$$

where $\tilde{K}^{\sigma}$ is a true material property, which is called the first effective bulk modulus of the material (Lomakin [*128*]). This modulus equals one ninth the sum of the nine normal stiffness matrix components C_{ijkl}:

$$\tilde{K}^{\sigma} = \frac{1}{9} \delta_{ij} C_{ijkl} \delta_{kl} = \frac{1}{9} \sum_{i=1}^{3} \sum_{j}^{3} C_{ij} \quad , \tag{56}$$

where C_{ij} are elements of the stiffness matrix (written in Voigt notation).

Alternately, the use of the deviatoric constitutive relation, equation 49, hinged upon the satisfaction of equation 48. Inverting equation 49 into compliance form and summing the three

equations for normal strain yields upon reduction

$$\sigma = \tilde{K}^{\epsilon} \left(\epsilon_{11} + \epsilon_{22} + \epsilon_{33} - \bar{e} \right) \quad , \tag{57}$$

where $\tilde{K}^{\epsilon}$ is a true material property, which is called the second effective bulk modulus of the material (Segletes [*34*]). This modulus equals the reciprocal of the sum of the nine normal compliance matrix components J_{ijkl}:

$$\tilde{K}^{\epsilon} = \frac{1}{\delta_{ij} J_{ijkl} \delta_{ij}} = \frac{1}{\sum_{i=1}^{3} \sum_{j=1}^{3} J_{ij}} \quad , \tag{58}$$

where J_{ij} are elements of the compliance matrix (written in Voigt notation). These effective moduli, unlike the bulk modulus, are independent of deviatoric stress in anisotropic materials. The first and second bulk moduli reduce to the conventional bulk modulus in the limit of isotropy. Once σ is known, the deviatoric stresses follow from equation 43.

It was mentioned previously that, for real materials under large compression, the empirical relation between dilatation and pressure is not a linear one and at high pressures is thermodynamically coupled to internal energy. One advantage of this deviatoric formulation lies in the ability to arbitrarily make the hydrostatic relations equations 57 and 58 nonlinear while retaining the linear simplicity of Hooke's Law for the deviatoric portion of the constitutive relation. Though this *ad hoc* procedure does not theoretically follow as an extension to Hooke's Law, it does permit the code user to more flexibly model the empirical EOS behavior of the material, as $-\sigma = p\left(\nu / \exp(\bar{e}), E\right)$. These tensors differ from the absolute stress / strain tensors in that the normal components of stress and strain are decremented by the hydrostatic values of the normal stresses and strains, respectively. In this way, the deviatoric quantities represent deviation from a hydrostatic condition, while the relationship existing between the average stress (negative of pressure) and hydrostatic strain (volumetric dilatation) is an EOS.

The approach proposed by Segletes (*34*), which was implemented as the transversely isotropic model in CTH (Taylor [*129*]), has found reflection in the modeling of an EOS for orthotropic materials proposed by Anderson *et al.* (*36*). At this point, the approach to describe an EOS for orthotropic materials proposed by Anderson *et al.* (*36*) is discussed. The final expression for the EOS (for the general orthotropic case) based on equations 5, 42, and 55, and proposed by

Anderson *et al.* (*36*), can be written in the following form:

$$\begin{aligned} p = P_H^A \cdot \left(1 - \frac{\Gamma}{2}\mu\right) + \rho\Gamma e \\ - \frac{1}{3\beta}\left\{E_x(1-\nu_{yz}\nu_{zy}) + E_x(\nu_{yx}+\nu_{zx}\nu_{yz}) + E_x(\nu_{zx}+\nu_{yx}\nu_{zy})\right\}\cdot\epsilon_{xx}^d - \\ - \frac{1}{3\beta}\left\{E_x(\nu_{yx}+\nu_{zx}\nu_{yz}) + E_y(1-\nu_{xz}\nu_{zx}) + E_y(\nu_{zy}+\nu_{xy}\nu_{zx})\right\}\cdot\epsilon_{yy}^d - \\ - \frac{1}{3\beta}\left\{E_x(\nu_{zx}+\nu_{yx}\nu_{zy}) + E_y(\nu_{zy}+\nu_{xy}\nu_{zx}) + E_z(1-\nu_{xy}\nu_{yx})\right\}\cdot\epsilon_{zz}^d \end{aligned} \quad , \tag{59}$$

where P_H^A is the anisotropic Hugoniot pressure. The first important difference between Anderson's and the conventional isotropic approach is in the way the Hugoniot pressure is approximated. The conventional approximation of the Hugoniot pressure P_H may assume cubic least squares curve fit in μ as

$$P_H = \begin{cases} A_1\mu + A_2\mu^2 + A_3\mu^3 & , \mu > 0 \\ A_1\mu \ , & \mu < 0 \end{cases} \quad , \tag{60}$$

where parameters $A_i, i = 1, 2, 3$ are determined by fit to experimental shock compression (Hugoniot) data. Note that for an isotropic material, A_1 is the bulk modulus. Anderson *et al.* (*36*) proposed that in order to have consistency and correct stresses in the elastic regime for an orthotropic material, the Hugoniot pressure P_H^A should be approximated as

$$P_H^A = \begin{cases} A_1'\mu + A_2\mu^2 + A_3\mu^3 & , \mu > 0 \\ A_1'\mu \ , & \mu < 0 \end{cases} \quad , \tag{61}$$

where A_1' is defined by the following quantity (Lomakin [*128*]; Anderson *et al.* [*36*]):

$$\begin{aligned} A_1' = \frac{1}{9\beta}\left(E_x(1-\nu_{yz}\nu_{zy}) + E_y(1-\nu_{xz}\nu_{zx}) + E_z(1-\nu_{xy}\nu_{yx})\right. \\ \left. + 2\cdot\left[E_x(\nu_{yx}+\nu_{zx}\nu_{yz}) + E_x(\nu_{zx}+\nu_{yx}\nu_{zy}) + E_y(\nu_{zy}+\nu_{zx}\nu_{xy})\right]\right) \end{aligned} \quad , \tag{62}$$

where $\beta = 1 - \nu_{xy}\nu_{yx} - \nu_{xz}\nu_{zx} - \nu_{yz}\nu_{zy} - 2\nu_{yx}\nu_{zy}\nu_{xz}$. Anderson *et al.* (*36*) interpreted A_1' as an "effective" or "average" bulk modulus $\tilde{K}^\sigma$ (first effective bulk modulus equation 56). It is important to note that expression for the EOS can likewise be obtained using equation 57, interpreting A_1' as the second effective bulk modulus. The A_2, A_3 parameters are determined from the fitting of the experimental data in all cases. This provides an appropriate description of material behavior at high pressures and reduces to the correct relations at small volumetric strains. Alternatively, A_1', A_2, A_3 can be analytically determined through a Taylor's series expansion of the Hugoniot pressure P. Assume that the linear approximation between the shock velocity U_S

and particle velocity u_p (equation 6, $S_2 = S_3 = 0$) exists, and that the U_S-u_p intercept c equals the ambient bulk speed of sound c_0. It follows that the Hugoniot curve and Taylor's series expansion of the Hugoniot pressure P with respect to μ can be written in the form

$$P_H^A = \frac{\rho_0 \cdot c_0^2 \cdot \mu \cdot (1+\mu)}{[1-\mu \cdot (S-1)]^2} \quad , \tag{63}$$

$$\begin{aligned} A_1' &= \rho_0 c_0^2 \\ A_2 &= A_1' \cdot [1 + 2(S-1)] \\ A_3 &= A_1' \cdot [2(S-1) + 3(S-1)^2] \\ U &= c_0 + S u_p \end{aligned} \quad , \tag{64}$$

where c_0, the ambient bulk speed of sound, has the following definition

$$c_0 = \sqrt{\frac{\tilde{K}^\sigma}{\rho_0}} \quad . \tag{65}$$

Some attempts to use Anderson's model to simulate the behavior of composite materials under shock loading have been made by Chen *et al.* (*130*), Hayhurst *et al.* (*131–133*), and Hiermaier *et al.* (*134*). The work of Hayhurst *et al.* (*131–133*) was directed towards numerical model development for the Nextel and Kevlar/Epoxy materials subject to hypervelocity impact. They also performed the experimental inverse flyer test (IFPT) for Nextel and Kevlar/Epoxy. Their models were to be macro-mechanically based and suitable for implementation into a hydrocode coupled with EOS. Each layer/weave of the material was not to be modeled explicitly but represented by an equivalent volume with properties on a macroscale, which are representative of the combined micro-mechanical response of the volume of the material under the loading conditions considered. The Kevlar/Epoxy IFPT experimental data and simulation results are presented in figure 4. A polynomial EOS, equations 59 and 60, was used in conjunction with damageable orthotropic stiffness. The samples recovered from impact tests gave evidence of phase changes during the impact events (figure 4). The Kevlar/Epoxy samples recovered after an impact at 572 m/s showed a reduced thickness with a residual bending strength. Separate Kevlar sheets were found in the impact vessel during impact test at 788 m/s. These Kevlar sheets showed a vanishing bending strength with all Epoxy impregnation to be evaporated. Impact test at 1015 m/s produced a fine Kevlar dust all over the impact vessel. At this impact velocity, Kevlar

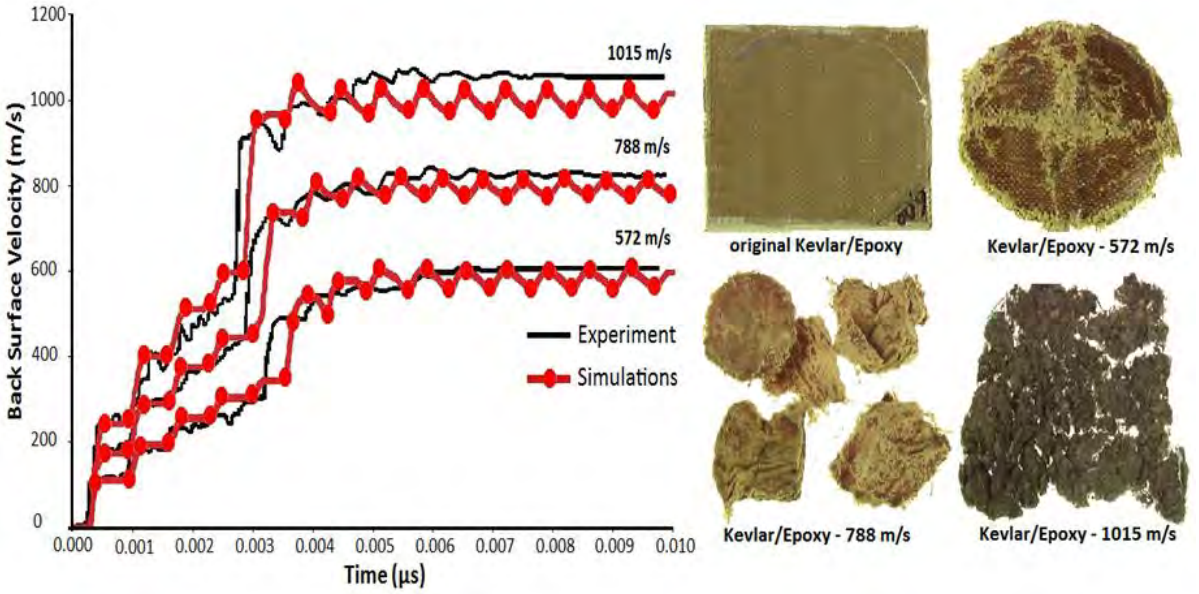

Figure 4. The Kevlar/Epoxy IFPT simulated and experimental back surface velocities for 572, 788, and 1015 m/s. The experimental data Kevlar/Epoxy materials recovered after flyer plate testing were taken from C. J. Hayhurst, *Multi-Physics Analysis of Hypervelocity Impact: Successes and Challenges*, FENET Presentation (Noordwjik, 2003) (*133*).

also undergoes a phase change of thermal decomposition. The weave and yarns decompose into a dark, wool-like material. It is important to note that the average slope of the initial rise in back surface velocity is well represented along with the sharp rise in velocity (figure 4) for all three impact velocities. The observed differences between the simulations and experiments can be attributed partly to the selected EOS approach and corresponding damage model (*i.e.*, compaction behavior and initial density). However, Hayhurst *et al.* (*131, 132*) models provide a significant improvement over the simulation with the standard orthotropic material models.

It was mentioned previously that in the case of an isotropic material, the hydrostatic stress (or pressure) induces a change of scale, while the deviatoric stress only induces a change of shape. It is obvious that in order to keep this property for anisotropic materials (*e.g.*, for orthotropic materials), the definition of "pressure" needs to be generalized, because a hydrostatic pressure (isotropic state of stress) applied to an anisotropic material results in an anisotropic state of strain. In other words, this loading will result not only in a change of scale, but also in change of shape. This is inconsistent with the definition of the "generalized pressure."

3.5 Generalized Decomposition of Anisotropic Constitutive Relationship Suitable for Shock-Wave Modeling

The definition of pressure equation 2 leads to the invariant quantity (the contraction of the stress tensor and the unit tensor is divided by the norm of the unit tensor). This is not the case when the pressure is defined as the portion of the mean stress that varies directly with the volumetric strain, which is not an invariant quantity (*i.e.*, this quantity cannot be expressed as contraction of the stress tensor and another second order tensor). However, the high-pressure thermodynamic EOS of anisotropic materials must be modified to account correctly for the elastic behavior at small volumetric strain. The generalized decomposition of the stress tensor was constructed by Lukyanov (*37–41, 135, 136*), assumed and given by the following theorem:

Theorem: *For anisotropic materials of any symmetry, where stress state and strain state are coupled via the generalized Hooke's law $\sigma_{ij} = C_{ijkl}\epsilon_{ij}$, $\epsilon_{ij} = J_{ijkl}\sigma_{ij}$ subject to the constraints for elements of stiffness and compliance matrixes (written in Voigt notation) such as*

$$\sum_{k=1}^{3} \left(C_{k1} + C_{k2} + C_{k3}\right)^2 \neq 0 \ , \quad \sum_{k=1}^{3} \left(J_{k1} + J_{k2} + J_{k3}\right)^2 \neq 0 \quad , \tag{66}$$

there is one and only one state of stress, $\tilde{\sigma}_{ij} = p\alpha_{ij}$, that results in only volumetric deformation, $\epsilon_{ij} = \epsilon_v \delta_{ij}$, as defined by the following decomposition:

$$\sigma_{ij} = -p^* \alpha_{ij} + \tilde{S}_{ij} \ , \quad p^* \alpha_{ij} \tilde{S}_{ij} = 0 \ , \quad \alpha_{ij}\alpha_{ij} = 3 \ , \quad \alpha_{ij} = 0 \ \forall \ i \neq j \quad , \tag{67}$$

$$p^* = p + p^{\tilde{S}} \ , \quad p = -\frac{\beta_{ij}\sigma_{ij}}{\beta_{kl}\alpha_{kl}} \ , \quad p^{\tilde{S}} = \frac{\beta_{ij}\tilde{S}_{ij}}{\beta_{kl}\alpha_{kl}} \ , \quad \tilde{\sigma}_{ij} = p\alpha_{ij} \quad , \tag{68}$$

where α_{ij} and β_{ij} are the first and second generalizations of the Kronecker delta symbol, p is the pressure related to the volumetric deformation, $p^{\tilde{S}}$ is the pressure related to the generalized deviatoric stress, p^* is the total generalized pressure, $\tilde{S}_{ij}$ is the generalized deviatoric stress tensor, $\epsilon_v = \epsilon_{ij}\delta_{ij}$ is the volumetric deformation, C_{ijkl} is the stiffness matrix, J_{ijkl} is the compliance matrix, $C_{ij} = C_{ji}$ are elements of the stiffness matrix (written in Voigt notation), and $J_{ij} = J_{ji}$ are elements of the compliance matrix (written in Voigt notation).

It is important to note that some attempts to construct generalized decomposition of stress tensor were made by Lomakin (*128*) and Sawyer (*137*). For anisotropic materials, the total hydrostatic "pressure" has been defined (*37–41, 135, 136*) and given as

$$p^* = p + \frac{\beta_{ij}\tilde{S}_{ij}}{\alpha_{ij}\beta_{ij}} \ , \quad p = -\frac{\beta_{ij}\sigma_{ij}}{\alpha_{ij}\beta_{ij}} \quad , \tag{69}$$

where p is the pressure related to the volumetric deformation and $\tilde{S}_{ij}$ is the generalized deviatoric part of the stress tensor. The relation equation 69 is the correct generalized "pressure" for the elastic regime. To provide an appropriate description of behavior for general anisotropic materials at high pressures, an EOS for p (pressure related to the volumetric deformation) has to be defined. The Mie-Grüneisen EOS equations 8 and 9 was used for p^{EOS} by Lukyanov (*37–41, 135, 136*) to describe the thermodynamic (EOS) material response, which also describes correctly the material's behavior at small volumetric strains. Therefore, an appropriate description of general hydrostatic "pressure" at high pressures has the following form:

$$p^{*} = p^{EOS} + \frac{\beta_{ij}\tilde{S}_{ij}}{\alpha_{ij}\beta_{ij}} \quad . \tag{70}$$

Note that the methodology described above can be applied for all anisotropic materials and represents a mathematically consistent generalization of the conventional isotropic case. The methodology for calculation of components of the tensor α_{ij} has been previously defined (*37–41, 135, 136*). The elements of tensor α_{ij} can be written in the following form:

$$\begin{aligned} \alpha_{11} &= (C_{11} + C_{12} + C_{13}) \cdot 3\bar{K}_C \\ \alpha_{22} &= (C_{12} + C_{22} + C_{23}) \cdot 3\bar{K}_C \\ \alpha_{33} &= (C_{13} + C_{23} + C_{33}) \cdot 3\bar{K}_C \end{aligned} \tag{71}$$

$$\bar{K}_C = 1/\sqrt{3 \cdot \left[(C_{11} + C_{12} + C_{13})^2 + (C_{12} + C_{22} + C_{23})^2 + (C_{13} + C_{23} + C_{33})^2\right]} \tag{72}$$

$$K_C = \frac{1}{9\bar{K}_C}$$

$$\alpha_{ij}\alpha_{ij} = \| \alpha \|^2 = 3 \quad , \tag{73}$$

where C_{ij} is the stiffness matrix (written in Voigt notation). The relation equation 73 describes the norm of tensor α_{ij}, which reduces to Kroncker's delta symbol norm in the limit of isotropy. Therefore, the norm of α_{ij} is taken to be $\sqrt{3}$. Furthermore, the following set of equations for the

components of the tensor β_{ij} can be written (Lukyanov [*37–41, 135, 136*]):

$$\beta_{11} = (J_{11} + J_{12} + J_{13}) \cdot 3K_S$$

$$\beta_{22} = (J_{12} + J_{22} + J_{23}) \cdot 3K_s$$

$$\beta_{33} = (J_{13} + J_{23} + J_{33}) \cdot 3K_s \qquad , \qquad (74)$$

$$K_s = 1/\sqrt{3 \cdot \left[(J_{11} + J_{12} + J_{13})^2 + (J_{12} + J_{22} + J_{23})^2 + (J_{13} + J_{23} + J_{33})^2\right]}$$

$$\beta_{ij}\beta_{ij} = \| \beta \|^2 = 3$$

where J_{ij} are elements of compliance matrix (written in Voigt notation). To be consistent with the definition of the bulk speed of sound c for isotropic material, the following definition

$$c = \sqrt{\frac{K_C}{\rho_0}} = c_0 \qquad (75)$$

is assumed for anisotropic bulk speed of sound. Here the first generalized bulk modulus K_C is defined according to equation 72. Based on methodology previously described, we can conclude that the two fundamental tensors α_{ij} and β_{ij}, which represent material properties, have been defined. Both of them can be considered as generalizations of the Kronecker delta symbol, which plays the main role in the theory of isotropic materials. Using two fundamental tensors α_{ij} and β_{ij}, the definitions of "total pressure" and pressure corresponding to the volumetric deformation can be defined. In the limit of isotropy, tensors α_{ij} andβ_{ij} have the following values $\alpha_{11} = \alpha_{22} = \alpha_{33} = 1$, $\beta_{11} = \beta_{22} = \beta_{33} = 1$ and the proposed generalization returns to the traditional classical case, where tensors α_{ij} and β_{ij} equal δ_{ij} and equations 67, 68, and 69 take the following form:

$$p^* = -\frac{\alpha_{ij}\sigma_{ij}}{\alpha_{ij}\alpha_{ij}} = -\frac{\sigma_{kk}}{3} \ , \ p = -\frac{\beta_{ij}\sigma_{ij}}{\beta_{ij}\alpha_{ij}} = -\frac{\sigma_{kk}}{3} \ , \ p^* = p \ , \ S_{ij} = \tilde{S}_{ij} = \sigma_{ij} - \delta_{ij} \cdot \frac{\sigma_{kk}}{3} \quad . \ (76)$$

Here, $p^* = p$ is the conventional hydrostatic pressure and S_{ij} is the conventional deviatoric stress tensor. Also, the two parameters K_c and K_s were considered as the first and second generalized bulk moduli. In the limit of isotropy they reduce to the well-known expression for the conventional bulk modulus $K = E/[3(1 - 2\nu)]$.

Most of the work discussing the response of composites to shock loading has examined the

material with the fiber plane normal to the loading axis (*e.g.*, Dandekar *et al.* [*13*], Zhuk *et al.* [*138*], Riedel *et al.* [*139*], Zaretsky *et al.* [*140*]). Overall, when shocked in this orientation, fiber-based composites appear to behave in a manner similar to monolithic polymers (*e.g.*, Carter *et al.* [*141*], Millett *et al.* [*142*]), indeed Zaretsky *et al.* (*140*) have made this point. The experimental study of a carbon fiber epoxy composite, shocking along the through-thickness orientation axis, showed no evidence of an inelastic deformation. Therefore, using an anisotropic nonlinear continuum framework and generalized decomposition of a stress tensor equations 66–73, shock-wave propagation in CFC materials was examined (Lukyanov [*41*]). The results of comparison between experimental data and numerical simulation are shown in the figure 5. The important characteristic, the arrival time to the Hugoniot stress level at the 0 mm position and back surface are in good correlation with experimental data. Further comparison shows that the pulse width and the reloading trace are in good agreement with the experimental data. The maximum difference between the experimental data and new proposed model for the plateau stress was 6%.

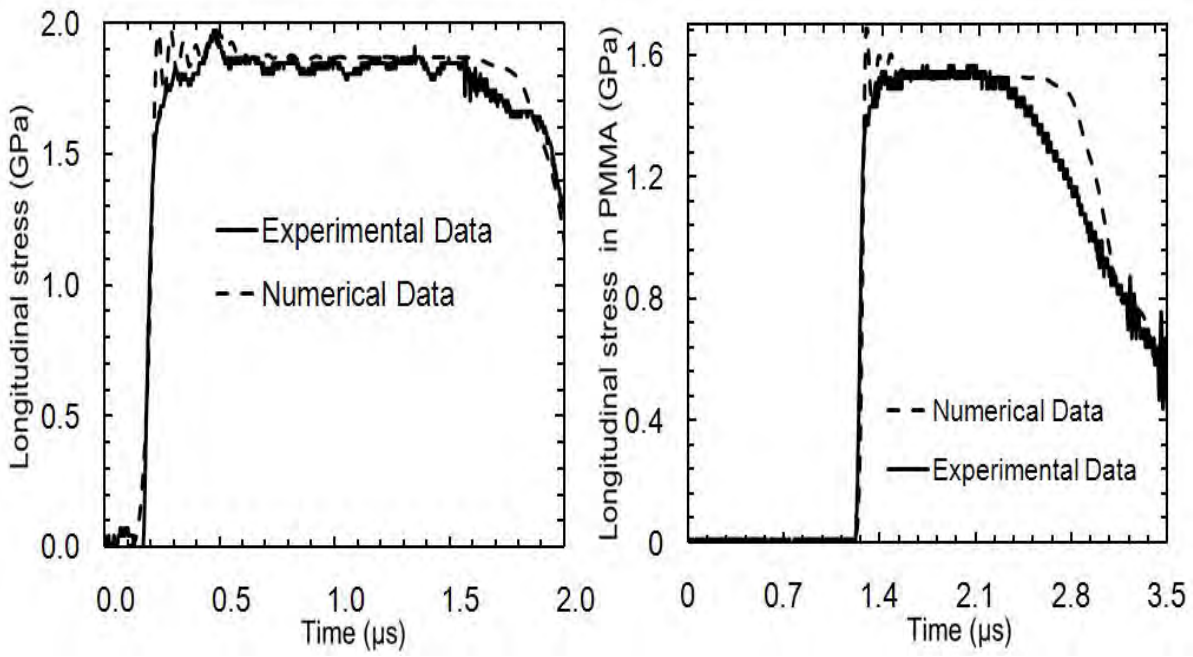

Figure 5. Representative experimental gauge traces from the through-thickness orientation at the 0 mm position and at the back surface, respectively (see Millett *et al.*) (*15*). The specimen was 3.8 mm thick. The impact conditions were a 5 mm dural flyer at $V = 504$ m/s. The dotted curve is the numerical data obtained using proposed damage model; the solid curve is the experimental data.

These experimental results show that the relationship between shock velocity and particle velocity through the thickness orientation is linear, yielding the relation (Millett *et al.* [*15*]):

$U_S^L = C_0^L + S_1^L u_p$, where $C_0^L = 3230$ m/s, $S_1^L = 0.92$. The experimental data in figure 6 are obtained for target plate thicknesses in the range between 2.3 and 5.7 mm (see Millett *et al.* [*15*]). It can be seen that there is a degree of scatter in this data. It was noticed that EOS data C_0^L and S_1^L are insensitive to thickness of the target plate over experimental range of the investigation (see Millett *et al.* [*15*]).

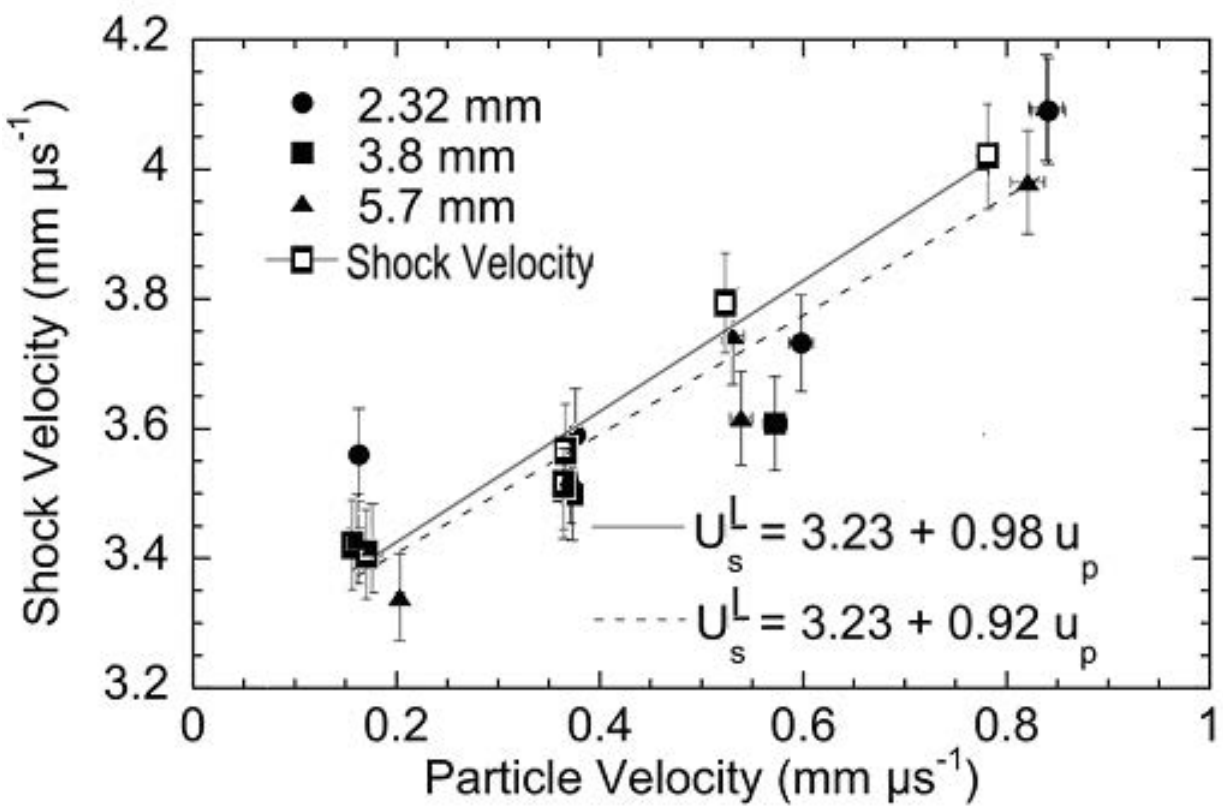

Figure 6. Experimental data U_S^L-u_p for the carbon-fiber-composite material, showing the variation with specimen thickness (experimental data obtained by Millett *et al.*) (*15*). The dotted curve is calculated using experimental data for U_S^L -u_p; the solid curve is calculated using numerical simulation based on the material model equations 66–73.

However, it would be expected that when the fiber direction is orientated along the impact axis, the response would be quite different. The results of Eden *et al.* (*90*) clearly differentiated between the response of the fibers and the matrix, indicating that the individual fibers were acting as wave-guides. Bordzilovsky *et al.* (*12*) examined the effects of orientation, with the orientation of the fibers ranging from 5° to 90° to the shock axis. Where the mis-orientation between fibers and the loading axis was small, a distinct low amplitude precursor wave was observed before arrival of the main shock. As the angle increased, the duration of this precursor decreased until it disappeared at 90°. This was interpreted as an elastic wave. Hereil *et al.* (*11*) observed similar

behavior in a three-dimensional carbon-carbon composite, with a low amplitude ramp preceding a much more quickly rising shock front. However, their interpretation suggested that this precursor was due to a high velocity wave transmitted along the fibers orientated in the shock axis, while the main shock was transmitted through the "matrix" (figure 7). Millett *et al.* (*15*) examined the carbon fiber-epoxy composite and obtained that the trace clearly has a ramped nature (figure 7), in common with the observations of Eden *et al.* (*90*) when using quartz stress gauges to measure the shape of the stress pulse in a similar orientation. This is qualitatively similar to the traces observed by Hereil *et al.* (*11*) and Bordzilovsky *et al.* (*12*), respectively.

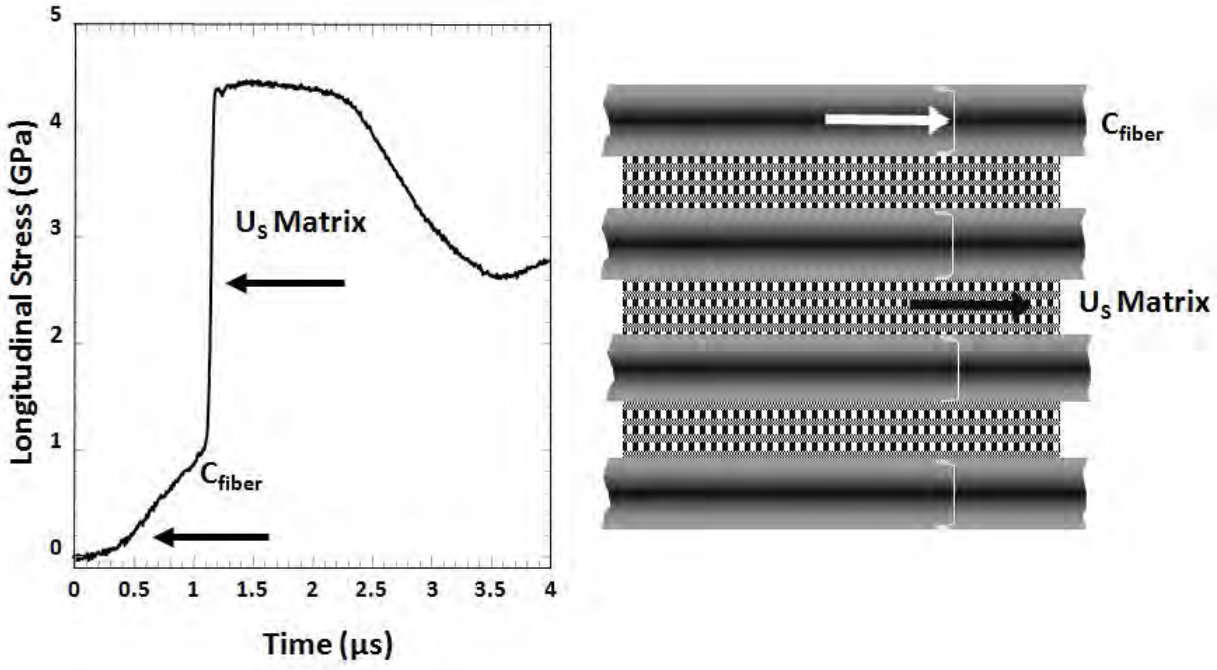

Figure 7. Representative experimental gauge traces from the fiber 0° orientation (see Millett *et al.*) (*15*). The specimen was 10 mm thick. The impact conditions were a 5 mm copper flyer at $V = 936$ m/s. According to Hereil *et al.* (*11*), the precursor was due to a high velocity wave transmitted along the fibers orientated in the shock axis, while the main shock was transmitted through the matrix.

It was pointed out by Bethe (*143*) that, for stable shock waves, the shock velocity must increase with pressure. This means that if the shock velocity should decrease with pressure, then the shock front would break up into two or more waves, or possibly one wave with a continuously smeared front. Note that the experimental data for the through thickness orientation (see, Lukyanov [*135*]) can be fitted by a linear relation, and there is no explicit evidence of the shock front breaking up; however, the analysis of the experimental data of Millett *et al.* (*15*) for selected CFC material shows that the shock velocity along the fiber 0° orientation decreases with pressure—therefore, a two-wave structure is proposed for describing the experimental data.

Furthermore, as the severity of the shock increases, the Hugoniot stress levels of the two orientations converge. This fact demonstrates that the selected CFC material shows isotropic behavior at high shock intensities, and can be described as an isotropic mixture of epoxy binder and fractured fibers (see, Lukyanov [*135*]). This is qualitatively similar to the Kevlar-Epoxy behavior observed by Hayhurst *et al.* (*131–133*) and Hiermaier *et al.* (*134*) (figure 4).

---

4. Anisotropic Plasticity Flow

The anisotropic material response under shock loading often shows inelastic (*e.g.*, plastic) deformation. The ability to predict inelastic response can be important for both ductile metals and relatively brittle composite materials. Note that even though composite materials are generally considered to be brittle, it is often prudent to use a small value for the equivalent plastic strain as a failure criterion (i.e., that point at which the material can no longer support shear and tensile stresses). Traditionally, the incremental strain of a material element is written as the sum of elastic and inelastic (*e.g.*, plastic) strains $\Delta\epsilon_{ij} = \Delta\epsilon^{e}_{ij} + \Delta\epsilon^{in}_{ij}$. Two types of inelastic deformation models, which do not result in loss of cohesion, are considered in the shock-wave modeling in anisotropic materials: an anisotropic-yield-criteria-based plasticity model (associated and non-associated) and a dislocation-based plasticity model.

4.1 Associated and Non-associated Anisotropic Plasticity

The main aspects of a phenomenological constitutive model can be characterized by a yield criterion representing a surface that separates the elastic and plastic regions of the stress space, a flow potential gradient that represents the direction of plastic strain rate, and a strain hardening rule. Generally, a yield function, a flow rule, and a set of evolution equations for M state variables are required to fully describe the constitutive relations of a plastic material. The yield function F for an anisotropic material in classical formulation can be expressed in the following general form:

$$\hat{F}(\sigma_{ij}, \gamma_k) = 0, \ k = 1, ..., M \quad . \tag{77}$$

Here σ_{ij} are the stress components and γ_k represents a set of state variables. The subscript k is introduced to indicate that there may be several state variables including the hardening parameters. When the material deforms plastically, the inelastic part of deformation (plastic

deformation) is defined by the flow rule

$$d\epsilon_{ij}^{p} = d\lambda \frac{\partial g}{\partial \sigma_{ij}} \quad , \tag{78}$$

where $g = g(\sigma_{ij}, \gamma_k)$ is the plastic potential, $d\epsilon_{ij}^{p}$ are the differentials of the plastic strain components, and $d\lambda$ is a positive scalar. In this study, we consider the associated plasticity flow models (*i.e.*, $\hat{F} = g$) and non-associated plasticity flow models (*i.e.*, $\hat{F} \neq g$). Finally, the evolution of M state variables can be described by

$$\alpha_k = A_k(d\epsilon_{ij}^{p}, \sigma_{ij}, \gamma_l) \quad , \quad k = 1, ..., M; \; l = 1, ..., M \quad . \tag{79}$$

For complex plasticity models, several evolution equations may be defined and the forms of these equations can be very complex.

Several anisotropic yield criteria and their associated yield surfaces have been developed in the past. These criteria have included a maximum stress law, a maximum strain law, and quadratic laws. One of the first yield conditions proposed for the anisotropic material is the quadratic yield criterions proposed by Dorn (*144*) and von Mises (Hill [*145*]) for plastically incompressible metal crystals with different lattice symmetry. In the theory of anisotropic yield criteria, the most well-known work is Hill's quadratic formulation (Hill [*145*]), which contains six parameters specifying the state of anisotropy, but is similar in form to the Mises's criterion for isotropic metals. From the literature review, a general group of anisotropic yield criteria suitable for anisotropic metals can be found. This group includes the yield conditions proposed by Bassani (*146*) and Hosford (*147*); the yield surface of four degrees specified by Gotoh (*148*) and Arminjon *et al.* (*149*); as well as yield surfaces of k degrees analyzed by Barlat and Lian (*150*), Barlat *et al.* (*151, 152*), Karafillis and Boyce (*153*), Barlat *et al.* (*154, 155*), Bron and Besson (*156*), Darrieulat and Montheillet (*157*), Stoughton and Yoon (*158*), Kowalczyk and Gambin (*159*), Hu (*160*), Hashiguchi (*161*), Hu (*162, 163*), and Barlat *et al.* (*164*). The quadratic laws are robust and are particularly well suited to multiaxial stress state. In particular, the Tsai-Hill theory (Hill [*145*]; Tsai and Hahn [*165*]) was considered by Segletes (*34*), Anderson *et al.* (*36*), and De Vuyst *et al.* (*166*).

Several models for inelastic deformation have been proposed based on generalized decomposition of stress tensor by Lomakin (*128*) and Sawyer (*137*). The mathematically consistent yield function of a fully anisotropic material based on generalized decomposition of the stress tensor into generalized spherical part (generalized hydrostatic pressure) and generalized deviatoric stress tensor equation 67 was proposed by Lukyanov (*37–41*). Based on research of Spitzig and

Richmond (*167*), Stoughton and Yoon (*158*) and generalized decomposition equation 67, the following yield function was used for modeling anisotropic elastic-plastic shock waves:

$$\hat{F}(\tilde{S}_{ij}) = \Psi(\tilde{S}_{ij})(1 + \chi\bar{p}^*) \leq Y(\bar{\epsilon}_p) \quad , \quad \bar{p}^* = \frac{\sigma_{ij}\alpha_{ij}}{\alpha_{kl}\alpha_{kl}} = \frac{1}{\| \alpha \|^2}\sigma_{ij}\alpha_{ij} \quad , \quad \bar{p}^* = -p^* \quad , \tag{80}$$

where $\bar{p}^*$ is the generalized hydrostatic stress and $\Psi(\tilde{S}_{ij})$ is described by generalized Hill's yield function:

$$\begin{aligned} \Psi^2(\tilde{S}_{ij}) = {} & F(\alpha_{33}\tilde{S}_{yy} - \alpha_{22}\tilde{S}_{zz})^2 + G(\alpha_{11}\tilde{S}_{zz} - \alpha_{33}\tilde{S}_{xx})^2 + H(\alpha_{22}\tilde{S}_{xx} - \alpha_{11}\tilde{S}_{yy})^2 \\ & + 2N\tilde{S}_{xy}^2 + 2L\tilde{S}_{yz}^2 + 2M\tilde{S}_{xz}^2 \end{aligned} \quad . \tag{81}$$

The material constants χ, F, G, H, N, L, and M are specified in terms of selected initial yield stresses in uniaxial tension, compression, and equibiaxial tension. It is worth noting that plasticity model equation 78 is naturally independent from the generalized hydrostatic stress $\bar{p}^* = (\sigma_{ij}\alpha_{ij})/(\alpha_{ij}\alpha_{ij})$, and therefore, the following equality can be written:

$$\Psi^2(\tilde{S}_{ij}) \equiv \Psi^2(\sigma_{ij}) \quad , \quad \sigma_{ij} = \bar{p}^*\alpha_{ij} + \tilde{S}_{ij} \quad , \quad \bar{p}^* \neq 0 \quad , \tag{82}$$

where $\tilde{S}_{ij}$ is the generalized deviatoric stress tensor and σ_{ij} is the stress tensor. This yield function was validated for a number of materials, *e.g.*, AA2008 T4, AA2090 T3, AA7108 T1, and AA6063 T1 (Lukyanov [*40*]). The shock-wave propagation in the anisotropic aluminum alloy 7010-T6 using the yield function equation 78 was performed by Lukyanov (*39*).

The experimental values, 0.39 and 0.33 GPa, for elastic response from the longitudinal and short transverse directions, respectively (figures 8 and 9), are in good correlation with the modeled values of the HEL longitudinal, 0.395 GPa, and short transverse, 0.333 GPa. The errors with respect to the experimental values are 1.4% and 0.9%, respectively, to the longitudinal and short transverse directions. Besides, other important characteristics, the arrival time to the HEL and the plastic wave velocity, are in good correlation with experimental data. Further comparison shows that the pulse width and the reloading trace are in good agreement with the experimental data (figures 8 and 9). The main conclusion obtained from these results is that the non-associated anisotropic plasticity model, as it stands, is suitable for simulating elasto-plastic wave propagation in anisotropic solids. Besides, different HELs are obtained when the material is impacted in different directions; their excellent agreement with the experiment demonstrates that the anisotropic plasticity model is adequate.

However, further work is required both in the experimental and constitutive modeling areas to find a better description of anisotropic material behavior.

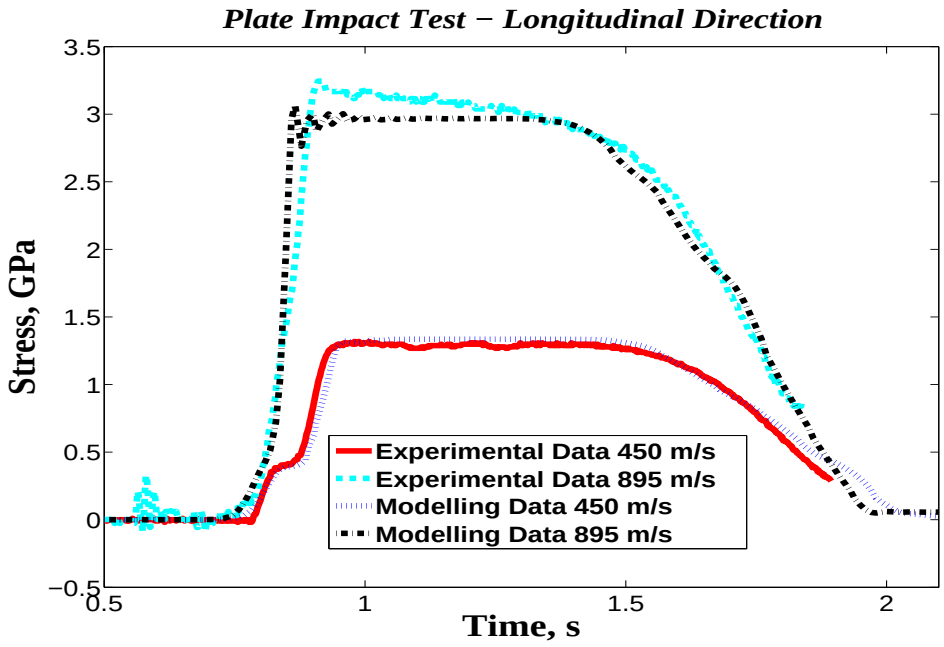

Figure 8. Back-surface gauge stress traces (longitudinal direction) from plate-impact experiments *vs.* numerical simulation of stress (PMMA) waves for plate impact tests (impact velocities 450 and 895 m/s) - target AA7010 T6.

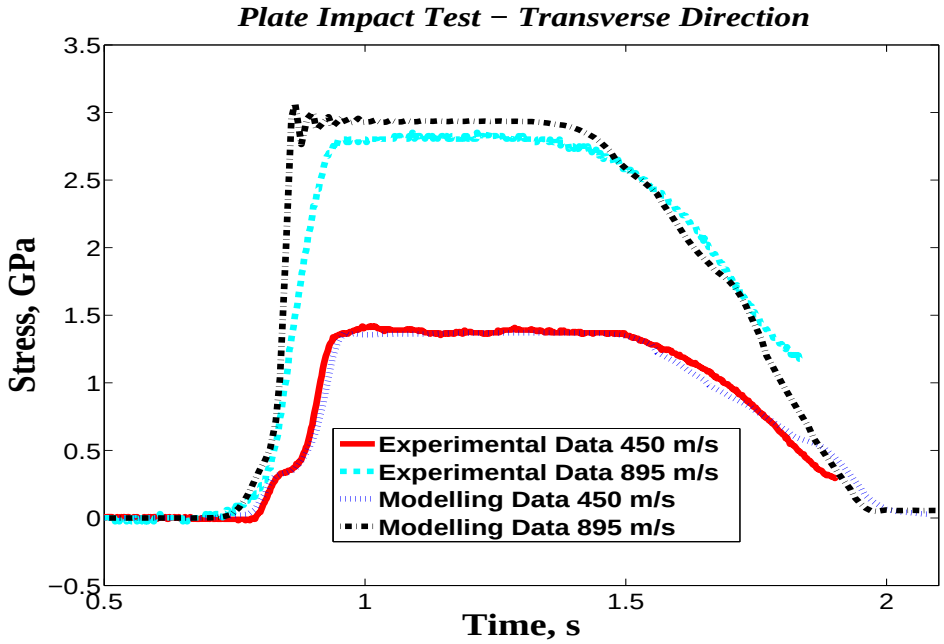

Figure 9. Back-surface gauge stress traces (transverse direction) from plate-impact experiments *vs.* numerical simulation of stress (PMMA) waves for plate impact tests (impact velocities 450 and 895 m/s) - target AA7010 T6.

4.2 Dislocation-based Plasticity

Much of the dislocation theory is now well established and is attributed to the early efforts of Taylor (*168*), Orowan (*169*), Gillis and Gilman (*170, 171*), and Gilman (*172, 173*). To incorporate dislocation-based plasticity, the Orowan equation (Gilman [*173*]; Winey and Gupta [*28, 29*]) is used to relate the motion of dislocations on a slip plane (denoted by α) to the plastic shear strain rate on that plane:

$$\dot{\gamma}_{\alpha}^{p} = N_{m}^{\alpha} b^{\alpha} \bar{V}^{\alpha} \quad , \tag{83}$$

where N_{m}^{α} is the mobile dislocation density operative on the slip plane, b^{α} is the magnitude of the Burgers vector, and $\bar{V}^{\alpha}$ is the average dislocation velocity. The incremental plastic strains in the coordinate system used to describe wave propagation are calculated by appropriately transforming and summing the plastic shear strains from all the individual slip systems (Winey and Gupta [*28–30*]):

$$\Delta\epsilon_{ij}^{p} = \frac{1}{2} \sum_{\alpha} \left(a_{1i}^{\alpha} a_{3j}^{\alpha} + a_{3i}^{\alpha} a_{1j}^{\alpha} \right) \dot{\gamma}_{\alpha}^{p} \Delta t \quad , \tag{84}$$

where Δt is the time step encountered in wave propagation calculation, and a_{ij}^{α} is the rotation matrix relating the coordinate system used to describe wave propagation to the slip plane coordinates. The resolved shear stress τ^{α} causing dislocation motion for a given slip system is determined by transforming the Cauchy stress from the coordinate system used to describe wave propagation to the slip plane coordinates system:

$$\tau^{\alpha} = \sigma_{13}^{\alpha} = a_{1i}^{\alpha} a_{3j}^{\alpha} \sigma_{ij} \quad . \tag{85}$$

To account for the rotation of slip planes due to finite elastic strains, the rotation matrices a_{ij}^{α} are updated each moment of time through a transformation that depends on the incremental elastic deformations (Winey and Gupta [*28–30*]). The dislocation-based models produce only shear strains, resulting in plastic incompressibility $D\epsilon_{kk}^{p} = 0$. The mobile dislocation density N_{m}^{α} and the average dislocation velocity $\bar{V}^{\alpha}$ must be defined in order to perform numerical simulations using equation 77. Winey and Gupta (*28–30*) employed a model (Gilman [*173*]) in which dislocations undergo regenerative multiplication under shock loading via a multiple cross glide mechanism. With this mechanism, the dislocation density is linearly related to the accumulated plastic shear strain γ_{α}^{p} (assumed positive)

$$N_{m}^{\alpha} = N_{m0} + M\gamma_{\alpha}^{p} \quad , \tag{86}$$

where N_{m0} is the initial density of mobile dislocations and M is the multiplication parameter.

The model also incorporates a stress-dependent dislocation velocity

$$\bar{V}^{\alpha} = \bar{V}_0 \exp\left[-D/\left(\tau^{\alpha} - \tau_0\right)\right] \quad , \tag{87}$$

where D is the drag stress parameter, τ^{α} is the resolved shear stress, τ_0 is the threshold stress for dislocation motion, and $\bar{V}_0$ is the shear wave speed. The dislocation-based plasticity model was used by Winey and Gupta (*29*) for a 6061-T6 aluminum plate impacting the LiF crystals at a velocity of *ca.* 0.34 km/s, where the target crystals are backed by a quartz stress gauge.

---

5. Early Anisotropic Implementations in Hydrocodes

Computational methods, as proposed by von Neumann (Clippinger [*174*]) came to the forefront with the advent of computers, beginning with the ENIAC, designed and built by the University of Pennsylvania (dedicated 1946) and installed at the United States Ballistic Research Laboratory in 1947 for the calculation of projectile trajectories (Bergin [*175*]). By the mid 1950s, newer generations of computers were fully engaged in computational fluid dynamics, *e.g.*, the particle-in-cell method (Evans and Harlow [*176*]).

By the early 1960s, the hydrocodes had evolved to model elasticity and radial-return (isotropic) plasticity (Wilkins [*102*]). It was not until the 1970s, though, that elastic and plastic transverse-isotropy were computationally implemented in the hydrocode framework of the HELP code (Sedgwick et al. [*177*]). Their formulation, however, cannot be termed deviatoric. The form of the relation used in HELP is

$$\Delta S_{ij} = C_{ijkl}\Delta\epsilon_{kl} - K(\Delta V/V)\delta_{ij} \quad , \tag{88}$$

where K is the bulk modulus, which presumably can be made dependent on dilatation (and therefore hydrostatic stress). In this way, the formulation may also provide the flexibility akin to a truly deviatoric formulation. However, equation 88 is not a deviatoric relation, since the deviatoric stress increment is not related to deviatoric strain increment, but rather is expressed in terms of the total strain increment. Similarly, the bulk modulus (as opposed to the effective bulk moduli derived in equations 56 and 58) is functionally dependent on deviatoric stress, and in this sense, equation 88 exhibits flawed behavior if the deviatoric variation in bulk modulus is not modeled. Finally, the flexibility afforded in equation 88 by allowing the bulk modulus to vary with hydrostatic stress has the disturbing effect that the resulting sum of the normal stress deviators is not generally zero. Thus, the use of the term "stress deviators" to describe the

left-hand side of equation 88 does not even seem justified.

The EPIC code added anisotropy in 1980 (Johnson *et al.* [*178*]) and uses a form similar to equation 88 except that K is defined in such a way as to force the sum of the normal stress deviators to zero. This *ad hoc* procedure will coincidentally mimic the behavior of equation 49, though the formulation is in error during the subsequent hydrostatic stress calculation by not accounting for the deviatorically induced dilatation $\bar{e}$ (see equation 46). In this sense, both the algorithms of HELP and EPIC introduced errors that were sensitive to the size of the hydrostatic strain increment (*i.e.*, the computational timestep) if variable compressibility were employed in the EOS. This problem was alleviated by the algorithm proposed by Segletes in 1987 (*34*), as described in section 3.4 of this report. Segletes' model was implemented into the Lagrangian DEFEL code and was used to study the effects of shear forming of copper liners upon the collapse of shaped-charge warheads (*179, 180*).

Some early computational implementations of anisotropy restricted themselves to linear elastic anisotropy, thereby limiting their application to dynamic problems involving gentle non-plastic impact. For example, the TIP code of Zak and Pillasch (*181*) is in this category, as well as the anisotropic implementation for the TOODY code by Swegle and Hicks (*182*). Zak (*183*) introduced anisotropic plasticity into the SANX code, thereby allowing calculation of a wider class of impact problems. With SANX, while the plasticity was anisotropic, the elasticity appears to be treated in an isotropic fashion. Later, the orthotropic elastic model was implemented into Lawrence Livermore National Laboratory (LLNL) DYNA3D and NIKE3D public domain codes (Hallquist and Whirley [*184*]; Maker *et al.* [*185*]), and in LS-DYNA commercial code (Hallquist [*186*]). In 1995, the CTH code of Sandia National Laboratories (Taylor [*129*]) incorporated the transversely isotropic model of Segletes (*34*) as its "TI model."

Nowadays, some models incorporate a user-defined subroutine within the commercial software (*e.g.*, ABAQUS) to take into account either a homogenous orthotropic model that examines the bulk macroscopic deformation response or the discrete non-homogeneous material distribution (Pankow *et al.* [*187*]). In such models, EOS does not even play a role. Rather, the volumetric treatment is one of a constant bulk modulus, insensitive to thermal effects.

Only recently, some attempts were made to properly account for nonlinear shock effects, energy dependence, and anisotropic stiffness in the existing hydrocodes. The approach, based on that by Anderson (*36*), has been incorporated into the AUTODYN hydrocode (Hayhurst [*131*]). The generalized decomposition of anisotropic constitutive relationship and EOS suitable for shock-wave modeling in anisotropic materials have been incorporated into the DYNA3D

hydrocode (Lukyanov [*38*]).

6. Conclusion

In the area of studies of materials under shock loading, barring a few, most of the studies are of a continuum nature. Therefore, the questions as to how shocks propagate and what the state of matter is immediately behind the shock front are pretty much open questions for anisotropic materials, though a few attempts have been made. It is expected that more experiments of shock-wave propagation will provide very valuable information. The plate impact tests in different directions at low and high intensities hold significant promise, particularly because of their one-dimensional planar shock-wave propagation and their time-resolved nature. Interaction of theory and experiment in this region may provide insight into the dynamic stress relation processes behind the shock front. The fact that the shock jump in pressure is essentially a nonequilibrium phenomenon may also play a deciding role. In the context of general shock-wave research, the measurement of precise temperature is a crying need. Presently, even the improved pyrometric method gives temperatures that are substantially higher than expected even at low pressure ranges. The area of study of kinetics of phase transitions of anisotropic materials under shocks is an interesting and challenging one, and some information could be derived from accurate experimental measurements. On the theoretical side, first-principle molecular dynamic calculation for anisotropic materials may contribute significantly to the understanding of shock propagation at high pressures. It can be hoped that this interaction of theory and experiments will open up new vistas in the area of high-pressure physics of anisotropic materials. Besides, there is an interesting possibility that the strain-rate sensitivity is itself orientation dependent in anisotropic materials. It has been noted for some anisotropic metals that the spall strengths are similar in both orientations at lower impact stresses, while at higher levels, the spall strength is higher in the longitudinal direction. This would seem to indicate a higher degree of strain-rate sensitivity in the longitudinal orientation, and would seem to agree with the observations made with the HELs for some anisotropic materials. Therefore, further development of the constitutive equations taking into account strain rate sensitivity is required.

Modern hydrocode shock modeling capabilities are confined almost exclusively to isotropic media; little provision has been made for anisotropic materials. In order to make numerical simulations of a hypervelocity impact on the reference configuration possible in terms of computation times, a macroscopic continuum model for the involved materials had to be developed. Due to the experimentally observed behavior of anisotropic materials, new

orthotropic hydrocode models were developed from the theoretical basis. This was necessary because total generalized pressure or conventional pressure inside these materials depends on deviatoric strain components as well as volumetric strain. Nonlinear effects, such as shock effects, can be incorporated through the volumetric straining in the material. Thus, a basis was found to couple the anisotropic material stiffness and strength with an anisotropic shock effects, associated energy dependence, and damage softening process. To our knowledge, this report presents the current state of the art in the experimental and theoretical developments of this fascinating field.

7. References

1. Wackerle, J. Shock-wave compression of quartz. *J. Appl. Phys.* **1962**, *33*, 922.

2. Zel'dovich, Y. B.; Raizer, Y. P. *Physics of Shock Waves and High-temperature Hydrodynamic Phenomena (vols. 1 and 2)*; Academic Press: New York, 1966.

3. Davison, L.; Graham, R. A. Shock compression of solids. *Phys. Rep.* **1979**, *55*, 255.

4. Eliezer, S.; Ghatak, A.; Hora, H.; Teller, E. *An Introduction to Equations of State, Theory and Applications*; Cambridge University Press: Cambridge, 1986.

5. Asay, J. R.; Shahinpoor, M. *High-Pressure Shock Compression of Solids*; Springer: New York, 1993.

6. Meyers, M. A. *Dynamic Behavior of Materials*; Wiley: New York, 1994.

7. Drumheller, D. S. *Introduction to Wave Propagation in Nonlinear Fluids and Solids*; Cambridge University Press: Cambridge, 1998.

8. Abrate, S. *Impact on Composite Structures*; Cambridge University Press: Cambridge, 1998.

9. Reid, S. R.; Zhou, G. *Impact Behaviour of Fibre-Reinforced Composite Materials*; Woodhead Publishing Ltd.: Cambridge, 2000.

10. Ryan, S.; Emi, F.; Thoma, K.; Hiermaier, S. *Hypervelocity Impact Induced Disturbances on Composite Sandwich Panel Spacecraft Structures*; Fraunhofer IRB Verlag: Stuttgart, 2008.

11. Hereil, P.-L.; Allix, O.; Gratton, M. Shock Behaviour of 3D Carbon-Carbon Composite. *J. Phys. IV* **1997**, *7*, 529.

12. Bordzilovsky, S. A.; Karakhanov, S. M.; Merzhievsky, L. A. Shock Response of a Unidirectional Composite at Various Orientations of Fibers. In *Shock compression of condensed matter—1997*; Schmidt, S. C., Dandekar, D. P., Forbes, J. W., Eds.; American Institute of Physics: Melville, New York, 1998.

13. Dandekar, D. P.; Hall, C. A.; Chhabildas, L. C.; Reinhart, W. D. Shock Response of a Glass Fiber-Reinforced Polymer Composite. *Compos. Struct.* **2003**, *61*, 51.

14. Espinosa, H.; Lu, H.-C.; Zavattieri, P.; Dwivedi, S. A 3-D Finite Deformation Anisotropic Visco-Plasticity Model for Fiber Composites. *J. Compos. Mater.* **2001**, *35* (5), 369.

15. Millett, J. C. F.; Bourne, N. K.; Meziere, Y. J. E.; Vignjevic, R.; Lukyanov, A. A. The Effect of Orientation on the Shock Response of a Carbon-Fiber Epoxy Composite. *Compos. Sci. Technol.* **2007**, *67* (15–16), 3253.

16. Aktaş, M.; Atas, C.; İçten, B. M.; Karakuzu, R. An Experimental Investigation of the Impact Response of Composite Laminates. *Compos. Struct.* **2009**, *87* (4), 307.

17. Hazell, P. J.; Appleby-Thomas, G. A Study On the Energy Dissipation of Several Different CFRP-based Targets Completely Penetrated by a High Velocity Projectile. *Compos. Struct.* **2009**, *91* (1), 103.

18. García-Castillo, S. K.; Sánchez-Sáez, S.; López-Puente, J.; Barbero, E.; Navarro, C. Impact Behaviour of Preloaded Glass/Polyester Woven Plates. *Compos. Sci. Technol.* **2009**, *69* (6), 711.

19. Tekalur, S. A.; Bogdanovich, A. E.; Shukla, A. Shock Loading Response of Sandwich Panels With 3-D Woven E-glass Composite Skins and Stitched Foam Core. *Compos. Sci. Technol.* **2009**, *69* (6), 736.

20. Butcher, B. M. *Spallation of 6061-T6 Aluminum: Behavior of Dense Media under High Dynamic Pressure*; Gordon and Breach: New York, 1968.

21. Johnson, J. N.; Barker, L. M. Dislocation Dynamics and Steady Plastic Wave Profiles in 6061-T6 Aluminum. *J. Appl. Phys.* **1969**, *40*, 4321.

22. Stevens, A. L.; Tuler, F. R. Effect of Shock Precompression on the Dynamic Fracture Strength of 1020 Steel and 6061-T6 Aluminum. *J. Appl. Phys.* **1971**, *42* (13), 5665.

23. Rosenberg, Z.; Luttwak, G.; Yesherun, Y.; Partom, Y. Spall Studies of Differently Treated 2024Al Specimen. *J. Appl. Phys.* **1983**, *54*, 2147.

24. Rosenberg, Z.; Yaziv, D.; Partom, Y. Calibration of Foil-Like Manganin Gauges in Planar Shock Wave Experiments. *J. Appl. Phys.* **1980**, *51*, 3702.

25. Gray III, G. T.; Bourne, N. K.; Zocher, M. A.; Maudlin, P. J.; Millett, J. C. F. Influence of Crystallographic Anisotropy on the Hopkinson Fracture "Spallation" of Zirconium. In *Shock Compression of Condensed Matter—1999*; Furnish, M. D., Chhabildas, L. C., Hixson, R. S., Eds.; American Institute of Physics: Woodbury, New York, 2000.

26. Gray III, G. T.; Lopez, M. F.; Bourne, N. K.; Millett, J. C. F.; Vecchio, K. S. Influence of Microstructural Anisotropy on the Spallation of 1080 Eutectoid Steel. In *Shock Compression of Condensed Matter—2001*; Furnish, M. D., Thadhani, N. N., Horie, Y., Eds.; American Institute of Physics: Melville, New York, 2002.

27. Rubin, M. B. Analysis of Weak Shocks in 6061-T6 Aluminum. In *Shock Waves in Condensed Matter—1989*; Schmidt, S. C., Johnson, J. N., Davison, L., Eds.; American Institute of Physics: New York, 1990.

28. Winey, J. M.; Gupta, Y. M. Nonlinear Anisotropic Description for Shocked Single Crystals: Thermoelastic Response and Pure Mode Wave Propagation. *J. Appl. Phys.* **2004**, *96* (4), 1993.

29. Winey, J. M.; Gupta, Y. M. Nonlinear Anisotropic Description for the Thermomechanical Response of Shocked Single Crystals: Inelastic Deformation. *J. Appl. Phys.* **2006**, *99*, 023510.

30. Winey, J. M.; Gupta, Y. M. Anisotropic Material Model and Wave Propagation Simulations for Shocked Pentaerythritol Tetranitrate Single Crystals. *J. Appl. Phys.* **2010**, *107*, 103505.

31. Johnson, J. N.; Jones, O.; Michaels, T. E. Dislocation Dynamics Dislocation Dynamics and Single-Crystal Constitutive Relations: Shock-Wave Propagation and Precursor Decay. *J. Appl. Phys.* **1970**, *41* (6), 2330.

32. Johnson, J. N. Propagation Produced by Planar Impact in Linearly Elastic Anisotropic Media. *J. Appl. Phys.* **1971**, *42*, 5522.

33. Johnson, J. N. Calculation of Plane-Wave Propagation in Anisotropic Elastic-Plastic Solids. *J. Appl. Phys.* **1972**, *43*, 2074.

34. Segletes, S. B. *Deviatoric Constitutive Relation for Anisotropic Materials*; BRL-TR-2825; U.S. Army Ballistic Research Laboratory: Aberdeen Proving Ground, MD, 1987.

35. O'Donoghue, P. E.; Anderson Jr., C. E.; Friesenhahn, G. J.; Parr, C. H. A Constitutive Formulation for Anisotropic Materials Suitable for Wave Propagation Computer Programs. *J. Compos. Mater.* **1992**, *26* (13), 1860.

36. Anderson Jr., C. E.; Cox, P. A.; Johnson, G. R.; Maudlin, P. J. A Constitutive Formulation for Anisotropic Materials Suitable for Wave Propagation Computer Program-II. *Comp. Mech.* **1994**, *15*, 201.

37. Lukyanov, A. A. Thermodynamically Consistent Anisotropic Plasticity Model. *Proc. IPC* **2006**, ISBN 0-7918-3788-2.

38. Lukyanov, A. A. Constitutive Behaviour of Anisotropic Materials under Shock Loading. *Int. J. Plasticity* **2008**, *24*, 140.

39. Lukyanov, A. A. An Equation of State for Anisotropic Solids under Shock Loading. *Eur. Phys. J. B.* **2008**, *64* (2), 159.

40. Lukyanov, A. A. Anisotropic Materials Behavior Modeling Under Shock Loading. *J. Appl. Mech.* **2009**, *76*, 061012.

41. Lukyanov, A. A. Shock Waves in Composite Materials. *Mech. Adv. Mat. and Struct.* **2010**, *17*, 304.

42. Barker, L. M.; Hollenbach, R. E. Laser Interferometer for Measuring High Velocities of any Reflecting Surface. *J. Appl. Phys.* **1972**, *43*, 4669.

43. Kanel, G. I. Some New Data on Deformation and Fracture of Solids under Shock-Wave Loading. *J. Mech. Phys. Solids* **1998**, *46* (10), 1869.

44. Kanel, G. I.; Baumung, K.; Bluhm, H.; Fortov, V. E. Possible Applications of the Ion Beams Technique for Investigations in the Field of Equation of State. *Nucl. Instr. and Meth. in Phys. Res. A* **1998**, *415* (3), 509.

45. Millett, J. C. F.; Bourne, N. K. Stress Measurements in a Shock Loaded Alumina: Shear Strength and Delayed Failure. *J. Mat. Sci.* **2001**, *36* (14), 3409.

46. Bourne, N. K.; Stevens, G. S. Gas Gun for Plane and Shear Loading of Inert and Explosive Targets. *Rev. Sci. Instrum.* **2001**, *72* (4), 2214.

47. Bourne, N. K. A 50 mm Bore Gas Gun for Dynamic Loading of Materials and Structures. *Meas. Sci. & Technol.* **2003**, *14*, 273.

48. Gu, Y. B.; Ravichandran, G. Dynamic Behavior of Selected Ceramic Powders. *Int. J. Impact Eng.* **2006**, *32*, 1768.

49. Steinberg, D. J. *Equation of State and Strength Properties of Selected Materials*; UCRL-MA-106439; Lawrence Livermore National Laboratory: Livermore, CA, 1991.

50. Johnson, J. N.; Hixson, R. S.; Gray III, G. T. Shock-Wave Compression and Release of Aluminum/Ceramic Composites. *J. Appl. Phys.* **1994**, *76*, 5706.

51. Kanel, G. I.; Razorenov, S. V.; Bogatch, A.; Utkin, A. V.; Grady, D. E. Simulation of Spall Fracture of Aluminum and Magnesium over a Wide Range of Load Duration and Temperature. *Int. J. Impact Eng.* **1997**, *20* (6–10), 467.

52. Millett, J. C. F.; Bourne, N. K.; Gray III, G. T. Behavior of the Shape Memory Alloy NiTi During One-Dimensional Shock Loading. *J. Appl. Phys.* **2002**, *92* (6), 3107.

53. Lopatnikov, S. L.; Gama, B. A.; Haque, J. M.; Krauthauser, C.; Gillespie Jr., J. W. High-Velocity Plate Impact of Metal Foams. *Int. J. Impact Eng.* **2004**, *30*, 421.

54. Zaretsky, E. B.; Kanel, G. I.; Razorenov, S. V.; Baumung, K. Impact Strength Properties of Nickel-Based Refractory Superalloys at Normal and Elevated Temperatures. *Int. J. Impact Eng.* **2005**, *31* (1), 41.

55. Gebbeken, N.; Greulich, S.; Pietzsch, A. Hugoniot Properties for Concrete Determined by Full-Scale Detonation Experiments and Flyer-Plate-Impact Tests. *Int. J. Impact Eng.* **2006**, *32*, 2017.

56. Bronkhorst, C. A.; Cerreta, E. K.; Xue, Q.; Maudlin, P. J.; Mason, T. A.; Gray III, G. T. An Experimental and Numerical Study of the Localization Behavior of Tantalum and Stainless Steel. *Int. J. Plasticity* **2006**, *22* (7), 1304.

57. Wallace, D. C. Nature of the Process of Overdriven Shocks in Metals. *Phys. Rev. B* **1981**, *24* (10), 5607.

58. Swegle, J. W.; Grady, D. E. Shock Viscosity and the Prediction of Shock Wave Rise Times. *J. Appl. Phys.* **1985**, *58* (2), 692.

59. Kanel, G. I.; Ivanov, M. F.; Parshikov, A. N. Computer Simulation of the Heterogeneous Materials Response to the Impact Loading. *Int. J. Impact Eng.* **1995**, *17*, 455.

60. Nellis, W. J.; Mitchell, A. C.; Young, D. A. Equation-of-state Measurements for Aluminum, Copper, and Tantalum in the Pressure Range 80-440 GPa (0.8-4.4 Mbar). *J. Appl. Phys.* **2003**, *93* (1), 304–310.

61. Bourne, N. K.; Gray III, G. T. Equation of State of Polytetrafluoroethylene. *J. Appl. Phys.* **2003**, *93* (11), 8966.

62. Krüger, L.; Meyer, L. W.; Razorenov, S. V.; Kanel, G. I. Investigation of Dynamic Flow and Strength Properties of Ti-6-22-22S at Normal and Elevated Temperatures. *Int. J. Impact Eng.* **2003**, *28* (8), 877.

63. Chijioke, A. D.; Nellis, W. J.; Silvera, I. F. High-Pressure Equations of State of Al, Cu, Ta, and W. *J. Appl. Phys.* **2005**, *98*, 073526.

64. Boidin, X.; Chevrier, P.; Klepaczko, J. R.; Sabar, H. Identification of Damage Mechanism and Validation of a Fracture Model Based on Mesoscale Approach in Spalling of Titanium Alloy. *Int. J. Solids Struct.* **2006**, *43*, 4595.

65. Petit, J.; Dequiedt, J. L. Constitutive Relations for Copper under Shock Wave Loading: Twinning Activation. *Mech. Mater.* **2006**, *38*, 173.

66. Whittier, J. S.; Peck, J. C. Experiments on Dispersive Pulse Propagation in Laminated Composites and Comparison with Theory. *J. Appl. Mech.* **1969**, *36*, 485; Trans. ASME, **91**, Series E.

67. Tauchert, T. R.; Guzelsu, A. N. An Experimental Study of Dispersion of Stress Waves in a Fiber-Reinforced Composite. *J. Appl. Mech.* **1972**, *39*, 98; Trans. ASME, **94**, Series E.

68. Asay, J. R.; Urzondowski, S. R.; Duenther, A. H. *Ultrasonic and Thermal Studies of Selected Plastics, Laminated Materials, and Metals*; AFWL-TR-67-91; Air Force Weapons Laboratory: Albuquerque, NM, 1968.

69. Mortimer, R. W.; Chou, P. C.; Rodini, B. T. In-Plane and Shear-Bending Impact of Laminated Composite Plates. *J. Appl. Mech.* **1976**, *43* (2), 275.

70. Chhabildas, L. C.; Swegle, J. W. Dynamic Pressure-Shear Loading of Materials using Anisotropic Crystals. *J. Appl. Phys.* **1980**, *51* (9), 4799.

71. Chhabildas, L. C.; Swegle, J. The Dynamical Response of Particulate-Loaded Materials. I. Pressure-Shear Loading of Alumina Particles in an Epoxy Matrix. *J. Appl. Phys.* **1982**, *53* (2), 954.

72. Jones, O. E.; Mote, J. D. Shock-Induced Dynamic Yielding in Copper Single Crystals. *J. Appl. Phys.* **1969**, *40* (12), 38.

73. Asay, J. R.; Fowles, G. R.; Durall, G. E.; Miles, M. H.; Tinder, R. F. Effects of Point Defects on Elastic Precursor Decay in LiF. *J. Appl. Phys.* **1972**, *43*, 2132.

74. Gupta, Y. M. Elastic Compression to 30 kbar along $\langle 111 \rangle$ in Shocked LiF. *J. Appl. Phys.* **1975**, *26* (2), 38.

75. Gupta, Y. M. Effect of Crystal Orientation on Dynamic Strength of LiF. *J. Appl. Phys.* **1977**, *48* (12), 5067.

76. Swearengen, J. C.; Lipkin, J.; Percival, C. M. Influence of Microstructure on the Dynamic High-Temperature Elastic Moduli of Aluminum. *J. Appl. Phys.* **1973**, *44* (12), 5209.

77. Halleck, P. M.; Wackerle, J. Dynamic Elastic-Plastic Properties of Single Crystal Pentaerythritol Tetranitrate. *J. Appl. Phys.* **1976**, *47* (3), 976.

78. Dick, J. J.; Ritchie, J. P. Molecular Mechanics Modeling of Shear and the Crystal Orientation Dependence of the Elastic Precursor Shock Strength in Pentaerythritol Tetranitrate. *J. Appl. Phys.* **1994**, *76* (5), 2726.

79. Nurick, G. N.; Langdon, G. S.; Chi, Y.; Jacob, N. Behaviour of Sandwich Panels Subjected to Intense Air Blast - Part 1: Experiments. *Compos. Struct.* **2009**, *91* (4), 433.

80. Iqbal, K.; Khan, S.-U.; Munir, A.; Kim, J.-K. Impact Damage Resistance of CFRP with Nanoclay Filled Epoxy Matrix. *Compos. Sci. Technol.* **2009**, *69* (11–12), 1949.

81. Enfedaque, A.; Molina-Aldareguía, J. M.; Gálvez, F.; González, C.; Llorca, J. Effect of Glass Fiber Hybridization on the Behavior Under Impact of Woven Carbon Fiber/Epoxy Laminates. *J. Compos. Mater.* **2010**, *44* (25), 3051.

82. Panahia, B.; Ghavanlooa, E.; Daneshmand, F. Transient Response of a Submerged Cylindrical Foam Core Sandwich Panel Subjected to Shock Loading. *Materials & Design* **2011**, *32* (5), 2611.

83. Jackson, M.; Shukla, A. Performance of Sandwich Composites Subjected to Sequential Impact and Air Blast Loading. *Composites Part B: Engineering* **2011**, *42* (2), 155.

84. Zhu, F.; Lu, G. A Review of Blast and Impact of Metallic and Sandwich Structures. *Electronic J. Struct. Engng* **2007**, *7*, 92.

85. Found, M. S.; Howard, I. C. Single and Multiple Impact Behaviour of a CFRP Laminate. *Compos. Struct.* **1995**, *32* (1–4), 159.

86. Delfosse, D.; Poursartip, A. Energy-Based Approach to Impact Damage in CFRP Laminates. *Composites Part A: Applied Science and Manufacturing* **1997**, *28* (7), 647.

87. David-Westa, O. S.; Nasha, D. H.; Banks, W. M. An Experimental Study of Damage Accumulation in Balanced CFRP Laminates Due to Repeated Impact. *Compos. Struct.* **2008**, *83* (3), 247.

88. Asay, J. R.; Vogler, T. J.; Ao, T.; Ding, J. L. Dynamic Yielding of Single Crystal Ta at Strain of 5×10^5 /s. *J. Appl. Phys.* **2008**, *109*, 073507.

89. Dlott, D. D. Developments in the Physical Chemistry of Shock Compression. *Annu. Rev. Phys. Chem.* **2011**, *62*, 575.

90. Eden, G.; Carden, M. H.; Collver, A. M.; Smith, C. P. M. Shock Wave Propagation in a 3-D Quartz Phenolic Composite. In *Shock compression of condensed matter—1989*; Schmidt, S., Johnson, J., Davison, L., Eds.; Elsevier Science Publishers B.V.: Amsterdam, 1990.

91. Walsh, J. M.; Christian, R. H. Equation of State from Shock Wave Measurements. *Phys. Rev.* **1955**, *97* (6), 1544.

92. McQueen, R. G.; Marsh, S. P. Equation of State for Nineteen Metallic Elements from Shock-Wave Measurements to Two Megabars. *J. Appl. Phys.* **1960**, *31* (7), 1253.

93. Thiel, M. V.; Kusubov, A. S.; Mitchell, A. C. (Eds.) *Compendium of Shock Wave Data*; UCRL 50108; Lawrence Radiation Laboratory: Livermore, CA, 1967.

94. Marsh, S. P. (Ed.) *LASL Shock Hugoniot Data*; University of California Press: Berkeley, 1980.

95. Trunin, R. F.; Gudarenko, L. F.; Zhernoklatov, M. V.; Simakov, G. V. *Experimental Data of Shock-Wave Compression and Adiabatic Expansion in Condensed Matter*; RFNC-VNIIEF: Sarov, Russia, 2001.

96. Kipp, M. E.; Grady, D. E. *Shock Compression and Release in High-Strength Ceramics*; SAND89-1461; Sandia National Laboratories: Albuquerque, NM, 1989.

97. Krivtsov, A. Between Spall Strength and Mesoparticle Velocity Dispersion. *Int. J. Impact Eng.* **1999**, *23*, 477.

98. Stoffel, M. An Experimental Method to Validate Viscoplastic Constitutive Equations in the Dynamic Response of Plates. *Mech. Mater.* **2005**, *37* (12), 1210.

99. Kiselev, A. B.; Lukyanov, A. A. Mathematical Modeling of Dynamic Processes of Irreversible Deforming, Micro- and Macrofracture of Solids and Structures. *Int. J. Forming Processes* **2002**, *5*, 359.

100. Kanel, G. I.; Razorenov, S. V.; Bogatch, A.; Utkin, A. V.; Fortov, V. E. Spall Fracture Properties of Aluminum and Magnesium at High Temperatures. *J. Appl. Phys.* **1996**, *79* (11), 8310.

101. Kanel, G. I.; Razorenov, S. V.; Utkin, A. V. Spallation in Solids under Shock-Wave Loading: Analysis of Dynamic Flow, Methodology of Measurements and Constitutive Factors. In *High pressure shock compression of solids II*; Davison, L., Grady, D. E., Mohsen, S., Eds.; Springer: Berlin, 1996.

102. Wilkins, M. L. *Calculation of Elastic-Plastic Flow*; UCRL-7322; University of California: Livermore, CA, 1963.

103. Kerley, G. I. *The Linear U_s-u_p Relation in Shock-Wave Physics*; Research Report KTS06-1; Kerley Technical Services: Appomattox, VA, 2006.

104. Segletes, S. B. Thermodynamic Stability of the Mie-Grüneisen Equation of State, and its Relevance to Hydrocode Computations. *J. Appl. Phys.* **1991**, *70* (5), 2489; (Erratum: 71(2), 1074).

105. Segletes, S. B. Further Examinations on the Thermodynamic Stability of the Mie-Grüneisen Equation of State. *J. Appl. Phys.* **1994**, *76* (8), 4560.

106. Segletes, S. B. The Effect of Thermodynamic Constraints upon the Mie-Grüneisen Equation of State. In *Constitutive Laws: Experiments and Numerical Implementation*; Rajendran, A. M., Batra, R. C., Eds.; CIMNE: Barcelona, 1995.

107. Segletes, S. B.; Walters, W. P. On Theories of the Grüneisen Parameter. *J. Phys. Chem. Solids* **1998**, *59* (3), 425.

108. Segletes, S. B. Vibrational Stiffness of an Atomic Lattice. In *Shock Compression of Condensed Matter—1999*; Furnish, M. D., Chhabildas, L. C., Hixson, R. S., Eds.; American Institute of Physics: New York, 1999.

109. Segletes, S. B. Classical Methods for Frequency-Based Equations of State. In *Recent Research Developments in Physics and Chemistry of Solids*; Vol. 1; Pandalai, S. G., Ed.; Transworld Research Network: Trivandrum, 2002; pp 1–26.

110. Dugdale, J. S.; MacDonald, D. K. C. The Thermal Expansion of Solids. *Phys. Rev.* **1953**, *89* (4), 832.

111. Benson, D. J. Computational Methods in Lagrangian and Eulerian Hydrocodes. *Comp. Meth. Appl. Mech. & Engng.* **1992**, *99*, 235.

112. Miller, G. H.; Colella, P. A High-Order Eulerian Godunov Method for Elastic-Plastic Flow in Solids. *J. Comput. Phys.* **2001**, *167*, 131.

113. Barton, P. T.; Drikakis, D.; Romenski, E. An Eulerian Finite-Volume Scheme for Large Elastoplastic Deformations in Solids. *Int. J. Numer. Meth. Eng.* **2010**, *81*, 453.

114. Dorovskii, V. N.; Iskol'dskii, A. M.; Romenskii, E. I. Dynamics of Impulsive Metal Heating by a Current and Electrical Explosion of Conductors. *J. Appl. Mech. Tech. Phys.* **1984**, *24*, 454.

115. Barton, P. T.; Drikakis, D. An Eulerian Method for Multi-Component Problems in Non-Linear Elasticity with Sliding Interfaces. *J. Comput. Phys.* **2010**, *229*, 5518.

116. Schreyer, H. L.; Maudlin, P. J. Thermodynamically Consistent Relations Involving Plasticity, Internal Energy and Thermal Effects. *Philos. T. Roy. Soc. A* **2010**, *363*, 2517.

117. Godunov, S. K.; Romenskii, E. I. Nonstationary Equations of Nonlinear Elasticity Theory in Eulerian Coordinates. *J. Appl. Mech. Tech. Phys.* **1972**, *13*, 868.

118. Kondaurov, V. I. Equations of Elastoviscoplastic Medium with Finite Deformations. *J. Appl. Mech. Tech. Phys.* **1982**, *23*, 584.

119. Plohr, B. J.; Sharp, D. H. A Conservative Formulation for Plasticity. *Adv. Appl. Math.* **1992**, *13*, 462.

120. Godunov, S. K.; Romenski, E. I. *Elements of Continuum Mechanics and Conservation Laws*; Kluwer Academic, Plenum Publishers: Dordrecht, New York, 2003.

121. Whitney, J. M.; Pagano, N. J. Shear Deformation in Heterogeneous Anisotropic Plates. *J. Appl. Mech.* **1970**, *37*, 1031; Trans. ASME, textbf92, Series E.

122. Wang, A. S. D.; Tuckmantel, D. L. Elastic Wave Surface in Heterogeneous Anisotropic Plates. *AIAA J.* **1973**, *11*, 1571.

123. Moon, F. C. Wave Surface Due to Impact on Anisotropic Plates. *J. Comp. Mat.* **1972**, *6*, 62.

124. Chow, T. S. On the Propagation of Flexural Waves in an Orthotropic Laminated Plate and Its Response to an Impulsive Load. *J. Comp. Mat.* **1971**, *5*, 319.

125. Sun, C. T.; Lai, R. Y. Exact and Approximate Analyses of Transient Wave Propagation in an Anisotropic Plate. *AIAA J.* **1974**, *12* (10), 1415.

126. Wallace, D. C. *Thermodynamics of Crystals*; Wiley: New York, 1972.

127. Wallace, D. C. Irreversible Thermodynamics of Flow in Solids. *Phys. Rev. B* **1980**, *22* (4), 1477.

128. Lomakin, V. About a Nonlinear Elasticity and Plasticity Theory of Anisotropic Media. *Proceedings of the Academy of Sciences of the USSR, Department of Technical Sciences* **1960**, *4*, 60; (in Russian).

129. Taylor, P. A. *CTH Reference Manual: The Transverse Isotropic (TI) Model*; SAND95-2750; Sandia National Laboratories: Albuquerque, NM, 1995.

130. Chen, J. K.; Allahdadi, A.; Carney, T. High-velocity Impact of Graphite/Epoxy Composite Laminates. *Compos. Sci. Technol.* **1997**, *57*, 1268.

131. Hayhurst, C. J.; Hiermaier, S. J.; Clegg, R. A.; Riedel, W.; Lambert, M. Development of Material Models for Nextel and Kevlar-Epoxy for High Pressures and Strain Rates. *Int. J. Impact Eng.* **1999**, *23* (1), 365.

132. Hayhurst, C. J.; Livingstone, I. H. G.; Clegg, R. A.; Destefanis, R.; Faraud, M. Ballistic Limit Evaluation of Advanced Shielding Using Numerical Simulations. *Int. J. Impact Eng.* **2001**, *26*, 309.

133. Hayhurst, C. J. Multi-Physics Analysis of Hypervelocity impact: Successes and Challenges; Presentation to FENet; NAFEMS: Noordwjik, 2003.

134. Hiermaier, S. J.; Riedel, W.; Hayhurst, C. J.; Clegg, R. A.; Wentzel, C. M. *Advanced Material Models for Hypervelocity Impact Simulations*; Report No. E 43/99; Ernst Mach Institut: Freiburg im Breisgau, Germany, 1999.

135. Lukyanov, A. A. An Equation of State of a Carbon-Fibre Epoxy Composite under Shock Loading. *Eur. Phys. J. B.* **2010**, *74*, 35.

136. Lukyanov, A. A. Comment on "Modeling Shock Waves in Orthotropic Elastic Materials". *J. Appl. Phys.* **2010**, *108*, 066102.

137. Sawyer, J. P. G.; Jones, R.; McKinlay, P. R. A Unified Constitutive Theory for Paper. *Compos. Struct.* **1998**, *42*, 93.

138. Zhuk, A. Z.; Kanel, G. I.; Lash, A. A. Glass-Epoxy Composite Behaviour under Shock Loading. *J. Phys. IV* **1994**, *4 (C8)*, 403.

139. Riedel, W.; Nahme, H.; Thoma, K. Equation of State Properties of Modern Composite Materials: Modeling Shock, Release and Spallation. In *Shock compression of condensed matter—2003*; Furnish, M. D., Gupta, Y. M., Forbes, J. W., Eds.; American Institute of Physics: Melville, New York, 2004.

140. Zaretsky, E.; deBotton, G.; Perl, M. The Response of a Glass Fibres Reinforced Epoxy Composite to an Impact Loading. *Int. J. Solids Struct.* **2004**, *41*, 569.

141. Carter, W. J.; Marsh, S. P. *Hugoniot equation of state of polymers*; LA-13006-MS; Los Alamos National Laboratory: Los Alamos, NM, 1995.

142. Millett, J. C. F.; Bourne, N. K.; Barnes, N. R. The Behaviour of an Epoxy Resin under One-Dimensional Shock Loading. *J. Appl. Phys.* **2002**, *92*, 6590.

143. Bethe, H. A. *The Theory of Shock Waves for Arbitrary Equation of State*; OSRD Rept. No. 545, serial No. 237; Office of Scientific Res. and Develop. 1942.

144. Dorn, J. E. Stress-Strain Relations for Anisotropic Plastic Flow. *J. Appl. Phys.* **1949**, *20*, 15.

145. Hill, R. *Mathematical Theory of Plasticity*; Clarendon Press: Oxford, 1950.

146. Bassani, J. L. Yield Characterization of Metals with Transversely Isotropic Plastic Properties. *Int. J. Mech. Sci.* **1977**, *19* (11), 651.

147. Hosford, W. F. Comments on Anisotropic Yield Criteria. *Int. J. Mech. Sci.* **1985**, *27* (7–8), 423.

148. Gotoh, M. A Theory of Plastic Anisotropy Based on a Yield Function of Fourth Order (Plane Stress State)—I/ II. *Int. J. Mech. Sci.* **1977**, *19* (9), 505 & 513.

149. Arminjon, M.; Bacroix, B.; Imbault, D.; Raphanel, J. A Fourth Order Plastic Potential for Anisotropic Metals and Its Analytical Calculation from the Texture Function. *Acta Mech.* **1994**, *107*, 33.

150. Barlat, F.; Lian, J. Plastic Behavior and Stretchability of Sheet Metals. Part I: A Yield Function for Orthotropic Sheet under Plane Stress Conditions. *Int. J. Plasticity* **1989**, *5* (1), 51.

151. Barlat, F.; Lege, D. J.; Brem, J. C. A Six-Component Yield Function for Anisotropic Materials. *Int. J. Plasticity* **1991**, *7* (7), 693.

152. Barlat, F.; Becker, R. C.; Hayashida, Y.; Maeda, Y.; Yanagawa, M.; Chung, K.; Brem, J. C.; Lege, D. J.; Matsui, K.; Murtha, S. J.; Hattori, S. Yielding Description of Solution Strengthened Aluminum Alloys. *Int. J. Plasticity* **1997**, *13* (4), 385.

153. Karafillis, A. P.; Boyce, M. C. A General Anisotropic Yield Criterion Using Bounds and a Transformation Weighting Tensor. *J. Mech. Phys. Solids* **1993**, *41* (12), 1859.

154. Barlat, F.; Maeda, Y.; Chung, K.; Yanagawa, M.; Brem, J. C.; Hayashida, Y.; Lege, D. J.; Matsui, K.; Murtha, S. J.; Hattori, S.; Becker, R. C.; Makosey, S. Yield Function Development for Aluminum Alloy Sheets. *J. Mech. Phys. Solids* **1997**, *45* (11–12), 1727.

155. Barlat, F.; Brem, J. C.; Yoon, J. W.; Chung, K.; Dick, R. E.; Lege, D. J.; Pourboghrat, F.; Choi, S.-H.; Chu, E. Plane Stress Yield Function for Aluminum Alloy Sheets—Part 1: Theory. *Int. J. Plasticity* **2003**, *19* (9), 1297.

156. Bron, F.; Besson, J. A Yield Function for Anisotropic Materials Application to Aluminum Alloys. *Int. J. Plasticity* **2004**, *20* (4–5), 937.

157. Darrieulat, M.; Montheillet, F. A Texture Based Continuum Approach for Predicting the Plastic Behaviour of Rolled Sheet. *Int. J. Plasticity* **2003**, *19* (4), 517.

158. Stoughton, T. B.; Yoon, J. W. A Pressure-Sensitive Yield Criterion under a Non-Associated Flow Rule for Sheet Metal Forming. *Int. J. Plasticity* **2004**, *20* (4–5), 705.

159. Kowalczyk, K.; Gambin, W. Model of Plastic Anisotropy Evolution with Texture-Dependent Yield Surface. *Int. J. Plasticity* **2004**, *20* (1), 19.

160. Hu, W. An Orthotropic Yield Criterion in a 3-D General Stress State. *Int. J. Plasticity* **2005**, *21* (9), 1771.

161. Hashiguchi, K. Generalized Plastic Flow Rule. *Int. J. Plasticity* **2005**, *21* (2), 321.

162. Hu, W. Constitutive Modeling of Orthotropic Sheet Metals by Presenting Hardening-Induced Anisotropy. *Int. J. Plasticity* **2007**, *23*, 620.

163. Hu, W. A Novel Quadratic Yield Model to Describe the Feature of Multi-Yield-Surface of Rolled Sheet Metals. *Int. J. Plasticity* **2007**, *23*, 2004.

164. Barlat, F.; Yoon, J. W.; Cazacu, O. On Linear Transformations of Stress Tensors for the Description of Plastic Anisotropy. *Int. J. Plasticity* **2007**, *23* (5), 876.

165. Tsai, S. W.; Hahn, H. T. *Introduction to composite materials*; Technomic Publishing Co.: Lancaster, PA, 1980.

166. De Vuyst, T.; Vignjevic, R.; Bourne, N. K.; Campbell, J. Modelling of Spall in an Anisotropic Aluminium Alloy. *Space Debris* **2000**, *2* (4), 225.

167. Spitzig, W. A.; Richmond, O. The Effect of Pressure on the Flow Stress of Metals. *Acta Metall.* **1984**, *32*, 457.

168. Taylor, G. I. The Mechanism of Plastic Deformation of Crystals. *Proc. R. Soc. Lond. A* **1934**, *145*, 362.

169. Orowan, E. Problems of Plastic Gliding. *Proc. Phys. Soc.* **1940**, *52*, 8.

170. Gillis, P. P.; Gilman, J. J. Dynamical Dislocation Theory of Crystal Plasticity. I. The Yield Stress. *J. Appl. Phys.* **1965**, *36*, 3370.

171. Gillis, P. P.; Gilman, J. J. Dynamical Dislocation Theory of Crystal Plasticity. II. Easy Glide and Strain Hardening. *J. Appl. Phys.* **1965**, *36*, 3380.

172. Gilman, J. J. Dislocation Dynamics and the Response of Materials to Impact. *Appl. Mech. Rev.* **1968**, *21*, 767.

173. Gilman, J. J. *Micromechanics of Flow in Solids*; McGraw-Hill: New York, 1969.

174. Clippinger, R. *A Logical Coding System Applied to the ENIAC (Electronic Numerical Integrator and Computer)*; Report No. 673; Ballistic Research Laboratories: Aberdeen Proving Ground, MD, 1948 (transcribed at http://ftp.arl.army.mil/tildemike/comphist/48eniac-coding/index.html).

175. Bergin, T. J. *50 Years of Army Computing: From ENIAC to MSRC*; ARL-SR-93; Army Research Laboratory: Aberdeen Proving Ground, MD, 2000.

176. Evans, M. W.; Harlow, F. H. *The Particle-in-Cell Method for Hydrodynamic Calculations*; LA-2139; University of California: Los Alamos, NM, 1957.

177. Sedgwick, R. T.; Waddell, J. L.; Hageman, L. J.; Gurtman, G. A.; Baker, M. *Influence of ABM Material Properties on Erosion Resulting from Particle Impact*; BRL-CR-322; Ballistic Research Laboratories: Aberdeen Proving Ground, MD, 1976.

178. Johnson, G. R.; Vavrick, D. J.; Colby, D. D. *Further Development of EPIC-3 for Anisotropy, Sliding Surfaces, Plotting, and Material Models*; ARBRL-CR-00429 (AD B048305L); Ballistic Research Laboratory: Aberdeen Proving Ground, MD, 1980.

179. Segletes, S. B. *Jet Rotation Resulting from Anisotropy of Shaped-Charge Liners*; Proc. Intl. Ballistic Symp.: Brussels, Belgium, 1989.

180. Segletes, S. B. *Mechanisms Inducing Jet Rotation in Shear-Formed Shaped-Charge Liners*; BRL-TR-3090; U.S. Army Ballistic Research Laboratory: Aberdeen Proving Ground, MD, 1990.

181. Zak, A. R.; Pillasch, D. W. *Finite Element Analysis of a Dynamically Loaded Flat Laminated Plate*; BRL-CR-00433; U.S. Army Ballistic Research Laboratory: Aberdeen Proving Ground, MD, 1980.

182. Swegle, J. W.; Hicks, D. L. *An Anisotropic Constitutive Equation for Use in Finite Difference Wave Propagation Calculations*; SAND-79-0382; Sandia National Laboratories: Albuquerque, NM, 1979.

183. Zak, A. R. *Finite Element Model for Nonaxisymmetric Structure with Rate-Dependent Yield Conditions*; ARBRL-CR-00524; U.S. Army Ballistic Research Laboratory: Aberdeen Proving Ground, MD, 1984.

184. Hallquist, J. O.; Whirley, R. G. *DYNA3D User manual, Nonlinear dynamic analysis in three dimensions*; UCID-19592, Rev. 5; Lawrence Livermore National Laboratory: Livermore, CA, 1989.

185. Maker, B. N.; Ferencz, R. M.; Hallquist, J. O. *NIKE3D: A Nonlinear, Implicit, Three-Dimensional Finite Element Code for Solid and Structural Mechanics - User's Manual*; Report UCRL-MA-105268; University of California, Lawrence Livermore National Laboratory: Livermore, CA, 1991.

186. Hallquist, J. O. *LS-DYNA Theoretical Manual*; Livermore Software Technology Corporation: Lawrence, CA, 1998.

187. Pankow, M.; Waas, A. M.; Yen, C.-F.; Ghiorse, S. Shock Loading of 3D Woven Composites: A Validated Finite Element Investigation. *Compos. Struct.* **2011**, *93* (5), 1347.

NO. OF COPIES	ORGANIZATION
1 (PDF ONLY)	DEFENSE TECHNICAL INFORMATION CTR DTIC OCA 8725 JOHN J KINGMAN RD STE 0944 FORT BELVOIR VA 22060-6218
1	DIRECTOR US ARMY RESEARCH LAB IMNE ALC HRR 2800 POWDER MILL RD ADELPHI MD 20783-1197
1	DIRECTOR US ARMY RESEARCH LAB RDRL CIO LT 2800 POWDER MILL RD ADELPHI MD 20783-1197
1	DIRECTOR US ARMY RESEARCH LAB RDRL CIO LL 2800 POWDER MILL RD ADELPHI MD 20783-1197
1	DIRECTOR US ARMY RESEARCH LAB RDRL D 2800 POWDER MILL RD ADELPHI MD 20783-1197

NO. OF COPIES	ORGANIZATION
1	AIR FORCE ARMAMENT LAB AFATL DLJR D LAMBERT EGLIN AFB FL 32542-6810
3	COMMANDER US ARMY ARDEC RDAR MEE W E BAKER A DANIELS R FONG B3022 PICATINNY ARSENAL NJ 07806-5000
2	COMMANDER US ARMY AVN & MISSILE CMD AMSAM RD PS WF S CORNELIUS S HOWARD REDSTONE ARSENAL AL 35898-5247
2	DARPA W SNOWDEN S WAX 3701 N FAIRFAX DR ARLINGTON VA 22203-1714
1	SANDIA NATIONAL LABORATORIES S SCHUMACHER PO BOX 5800 ALBUQUERQUE NM 87185-MS0836
9	LLNL R E TIPTON L-095 D BAUM L-163 M MURPHY L-099 T MCABEE L-095 G POMYKAL L-072 J E REAUGH L-282 R M KUKLO L-099 G SIMONSON L-099 R BARKER L-020 PO BOX 808 LIVERMORE CA 94550
5	LOS ALAMOS NATL LABORATORY L HULL MS A133 C WINGATE MS D413 C RAGAN MS D449 E J CHAPYAK MS F664 J BOLSTAD MS G787 PO BOX 1663 LOS ALAMOS NM 87545
3	SOUTHWEST RESEARCH INST C ANDERSON S A MULLIN J WALKER PO DRAWER 28510 SAN ANTONIO TX 78228-0510
3	DE TECHNOLOGIES R CICCARELLI W FLIS W CLARK 100 QUEENS DR KING OF PRUSSIA PA 19406
1	DREXEL UNIVERSITY MEM DEPT B FAROUK 32ND & CHESTNUT ST PHILADELPHIA PA 19104
1	VIRGINIA POLYTECHNIC INSTITUTE COLLEGE OF ENGINEERING DEPT ENGNG SCI & MECHANICS R C BATRA BLACKSBURG VA 24061-0219
1	KERLEY PUBLISHING SERVICES G I KERLEY PO BOX 709 APPOMATOX VA 24522-0709
1	TEXTRON DEFNS SYS C MILLER 201 LOWELL ST WILMINGTON MA 01887-4113
1	LOCKHEED MARTIN ELECT & MIS G W BROOKS 5600 SAND LAKE RD MP 544 ORLANDO FL 32819-8907

NO. OF COPIES	ORGANIZATION
2	GD OTS D BOEKA N OUYE 2950 MERCED ST STE 131 SAN LEANDRO CA 94577
1	JAMS PROJECT OFFICE ATTN: SFAE-MSLS-JAMS-SYS-O C ALLEN 5250 MARTIN RD REDSTONE ARSENAL AL 35898
1	HALLIBURTON ENERGY SVCS JET RESEARCH CTR D LEIDEL PO BOX 327 ALVARADO TX 76009-9775
1	GEN CORP AEROJET D PILLASCH B57 D3700 1100 W HOLLYVALE ST AZUSA CA 91702
1	INTRNTL RSRCH ASSOC D ORPHAL 4450 BLACK AVE PLEASANTON CA 94566-6105

NO. OF COPIES	ORGANIZATION
	ABERDEEN PROVING GROUND
77	DIR USARL RDRL SL P TANENBAUM RDRL SLB R BOWEN RDRL SLB D R GROTE L MOSS J POLESNE RDRL SLB E M PERRY C BARKER D FORDYCE P HORTON D HOWLE D LYNCH M MAHAFFEY R SAUCIER RDRL SLB G P MERGLER RDRL SLB S R BOWERS M OMALLEY RDRL SLB W L ROACH J ABELL W MERMAGEN RDRL WM P PLOSTINS RDRL WMS T ROSENBERGER RDRL WML M ZOLTOSKI RDRL WML C K MCNESBY RDRL WML H T EHLERS T FARRAND E KENNEDY L MAGNESS C MEYER B SORENSEN R SUMMERS RDRL WMM B G GAZONAS RDRL WMP P BAKER S SCHOENFELD

NO. OF
COPIES ORGANIZATION

RDRL WMP A
A PORWITZKY
RDRL WMP B
C HOPPEL
R KRAFT
S SATAPATHY
M SCHEIDLER
RDRL WMP C
T BJERKE
J BARB
R BECKER
S R BILYK
N BRUCHEY
D CASEM
J CLAYTON
D DANDEKAR
T DIGLIANI
M GREENFIELD
B LEAVY
S SEGLETES (5 COPIES)
C WILLIAMS
RDRL WMP D
J RUNYEON
R FREY
D KLEPONIS
H W MEYER
R MUDD
B SCOTT
K STOFFEL
W WALTERS
RDRL WMP E
M BURKINS
W A GOOCH
D HORNBAKER
E HORWATH
B LOVE
RDRL WMP F
N GNIAZDOWSKI
R BITTING
E FIORAVANTE
R GUPTA
RDRL WMP G
N ELDREDGE
W BUKOWSKI
R EHLERS
B KRZEWINSKI
S KUKUCK

NO. OF COPIES	ORGANIZATION
1	A. LUKYANOV ABINGDON TECHNOLOGY CENTRE SCHLUMBERGER ABINGDON OX14 1UJ UNITED KINGDOM
1	E ROMENSKI SOBOLEV INSTITUTE OF MATHEMATICS SB RAS NOVOSIBIRSK 630090 RUSSIA
1	S SCHMAUDER INST MATERIALS TESTING, MATERIALS SCIENCE AND STRENGTH OF MATERIALS UNIVERSITY OF STUTTGART PFAFFENWALDRING 32 D-70569 STUTTGART GERMANY
1	V PETROVA DEPARTMENT OF MATHEMATICS VORONEZH STATE UNIVERSITY UNIVERSITY SQ 1 VORONEZH 394006 RUSSIA
1	J C F MILLETT DEPARTMENT OF HYDRODYNAMICS AWE ALDERMASTON READING RG7 4 PR UNITED KINGDOM
1	ST. PETERSBURG STATE TECHNICAL UNIVERSITY FACULTY OF PHYS AND MECHANICS DEPT OF THEORETICAL MECHANICS ATTN: A M KRIVTSOV POLITECHNICHESKAYA STREET 29 195251 ST-PETERSBURG RUSSIA
2	RUSSIAN FEDERAL NUCLEAR CENTER - VNIIEF L F GUDARENKO R F TRUNIN MIRA AVE., 37 SAROV 607190 RUSSIA

NO. OF COPIES	ORGANIZATION
1	ROYAL MILITARY ACADEMY G DYCKMANS RENAISSANCELAAN 30 1000 BRUSSELS BELGIUM
1	NORDMETALL GMBH L W MEYER EIBENBERG EINSIEDLER STR 18 H D-09235 BURKHARDTSDORF GERMANY
2	TU CHEMNITZ L W MEYER (x2) FAKULTAET FUER MASCHINENBAU LEHRSTUHL WERKSTOFFE DES MASCHINENBAUS D-09107 CHEMNITZ GERMANY
4	INSTITUTE OF CHEMICAL PHYSICS RUSSIAN ACADEMY OF SCIENCES G I KANEL A M MOLODETS S V RAZORENOV A V UTKIN 142432 CHERNOGOLOVKA MOSCOW REGION RUSSIA
3	INSTITUTE OF MECH ENGINEERING PROBLEMS V BULATOV D INDEITSEV Y MESCHERYAKOV BOLSHOY, 61, V.O. ST PETERSBURG 199178 RUSSIA
1	SAMARA STATE AEROSPACE UNIV L G LUKASHEV SAMARA RUSSIA
1	TOMSK STATE UNIVERSITY A G GERASIMOV 5-TH ARMY STREET, 29-61 TOMSK 634024 RUSSIA

NO. OF COPIES	ORGANIZATION
1	DEFENCE SCIENCE & TECH LAB PHYSICAL SCIENCES DEPT D POPE PORTON DOWN SALISBURY SP4 0JQ UNITED KINGDOM